

# Application of machine learning into organic Rankine cycle for prediction and optimization of thermal and exergy efficiency

Wei Wang, Shuai Deng, Dongpeng Zhao, Li Zhao\*, Shan Lin, Mengchao Chen

*Key Laboratory of Efficient Utilization of Low and Medium Grade Energy (Tianjin University), MOE, Tianjin 300350, China*



## ARTICLE INFO

**Keywords:**

Organic Rankine cycle  
Machine learning  
Back Propagation Neural Network  
Support Vector Regression  
Prediction  
Optimization

## ABSTRACT

Organic Rankine cycle (ORC) is a promising technology to recovery and utilization of low grade thermal energy. In recent years, there are few researches on ORC performance prediction based on Machine Learning, mainly due to a lack of reasonable methodology and case demonstration. This paper presented a comprehensive method to achieve a reasonable application of Machine Learning into ORC research for prediction and optimization of ORC's parameter and performance. Firstly, a cycle database was established by thermodynamic modeling, including four ORC configurations and seven working fluids. Then, for Machine Learning, the Back Propagation Neural Network (BPNN) and Support Vector Regression (SVR) prediction models for ORC were built by predicting error analysis with part of the database which can determine the best parameters of BPNN and SVR. Finally, taking RORC as example, cycle parameter analysis and multi-objective optimization of ORC were conducted based on the thermodynamic model and prediction model to maximize the thermal and exergy efficiency simultaneously. By the prediction and optimization results, it can be deserved that the accurate and fast prediction of the thermal efficiency and exergy efficiency of ORC with multi-parameter, multi-configuration and multi-working fluid was realized, and the optimization results based on the prediction model as the proxy model were also greatly close to the traditional optimization results based on the thermodynamic model. It should be noted that the comprehensive performance of prediction and optimization will be better with more data input. In conclusion, considering accuracy, calculation time, economic cost and safety, the ORC prediction and optimization method proposed in this paper is a promising technology combining Machine Learning and energy utilization, which could provide a new perspective for research in this field.

## 1. Introduction

In recent years, due to the increasingly severe energy and environment situation, energy saving and emission reduction have been paid more and more attention. Low grade [1] waste heat energy is an important part of energy recovery and utilization. Its common recycling ways include organic Rankin cycle (ORC) [2], Kalina cycle [3], Brayton cycle [4], absorption refrigeration cycle [5], Stirling cycle [6], ejection compression refrigeration cycle [7] and other thermodynamic cycle systems. Among them, ORC, as a typical waste heat power generation technology, has been widely studied and applied because of its advantages of high efficiency, simple configuration, safety and reliability and low investment cost [8–10].

Therefore, the optimization of ORC system has become an international hot research topic in recent years. At present, most of the researches of ORC are based on specific experiment [11–13] and modeling calculation [14–17]. Ziviani et al. [18] established a ORC unit to

evaluate the influence of the expander performance on the behavior of the ORC system based on the experimental data, and achieved the optimization of the operation of the ORC unit with R245fa finally. Yang et al. [19] proposed a new refrigerant R1233zd(E) with extremely low GWP as an environmental friendly substitute of R245fa, and then an experiment was carried out under a design of extensive operating conditions to compare the results between two refrigerants. Afterwards, R1233zd(E) was proven as an appropriate alternative to R245fa based on the study. Ghasemian et al. [20] discussed subcritical organic Rankine cycle for eight working fluids from the view of thermodynamics and economics based on thermodynamic modeling. Considering the thermal efficiency, exergy efficiency and cost of energy production, R11 in all working fluids showed the best performance. Bao, et al. [21] proposed a superstructure based on the mathematical model of the three-stage condensation Rankine cycle to achieve the simultaneous optimization of cycle parameters, structures and working fluids. Sun et al. [22] derived and optimized the performance analytical function

\* Corresponding author.

E-mail address: [jons@tju.edu.cn](mailto:jons@tju.edu.cn) (L. Zhao).

<b>Nomenclature</b>			
<i>T</i>	temperature(K)	R114	1,2-dichloro-1,1,2,2-tetrafluoroethane
<i>P</i>	pressure(kPa)	R11	trichlorofluoromethane
<i>H</i>	enthalpy(kJ/kg)	R1234ze(E)	trans-1,3,3,3-tetrafluoropropene
<i>m</i>	mass flow rate (kg/s)	MSE	mean squared error
<i>Q</i>	heat transfer rate (W)	MAE	mean absolute error
<i>W</i>	work transfer rate (W)	MRE	mean relative error
<i>E</i>	exergy transfer rate(W)	R <sup>2</sup>	determination coefficient
<i>y</i>	output value	ODP	ozone depression potential
<i>Greek letters</i>		GWP	global warming potential
$\eta$	efficiency	<i>Subscripts</i>	
$\lambda$	reheat pressure ratio	th	thermal
<i>Abbreviations</i>		ex	exergy
ORC	organic Rankine cycle	t	turbine
BPNN	Back Propagation Neural Network	p	pump
SVR	Support Vector Regression	con	condenser
SVM	Support Vector Machine	eva	evaporator
BORC	basic organic Rankine cycle	r	reheater
RORC	reheating organic Rankine cycle	ir	internal regenerator
IORC	internal regenerative organic Rankine cycle	tur	turbine
CRIORC	combined reheating-internal regenerative organic Rankine cycle	pump	pump
R141b	1,1-dichloro-1-fluoroethane	c	critical
R236ea	1,1,1,2,3,3-hexafluoropropane	b	boiling
R245fa	1,1,1,3,3-pentafluoropropane	0	atmospheric state
R245ca	1,1,2,2,3-pentafluoropropane	ppe	pinch point temperature in the evaporator
R123	2,2-dichloro-1,1,1-trifluoroethane	sh	superheat
		sc	supercooling
		f	working fluid
		1,2,2',2'',3,4,4'4'',2s,4s,a,b,as	state points of working fluid

and exergy efficiency of ORC in ocean thermal energy conversion, and results showed that ammonia is a good choice for ORC utilized in ocean thermal energy conversion from net power output viewpoint. In addition, ORC could also be integrated with other cycles to combine the cycles' structures and improve the energy recycle, which could increase its thermodynamic efficiency, such as the integration of ORC with Brayton cycle [23,24], Stirling cycle [25], etc.

As these above works of ORC, most of researches in recent decades are based on traditional methods of the specific experiment and thermodynamic modeling whose workload and the cost involved are relatively large in solving large-scale problems, although the research results have high accuracy. While guaranteeing the certain accuracy of the results, we try to find an economical and effective method which could quickly solve the calculation problem of various performance indices of ORC system. This method should have the certain accuracy and working speed, and make an appropriate trade-off between them. With the rise and development of artificial intelligence in recent years, there is a new way to solve this problem. Therefore, this paper proposed a method to achieve the performance prediction, parameter analysis and optimization based on Machine Learning. The idea of the approach came from that Borboudakis et al. [26] used machine learning to predict the chemical properties of MOF materials, Meng et al. [27] used Back Propagation Neural Network (BPNN) to predict the performance of the heat exchanger, etc. At present, there are few studies related to ORC performance prediction. Zhi, et al. [28] established an artificial neural network model to accurately predict the optimal cycle high pressure and thermal efficiency of transcritical ORC for R1234ze(E) working fluid. Yang et al. [29] used BPNN to predict and optimize the

output power and the evaporator outlet exhaust temperature of ORC system for diesel engine waste heat recovery. Dong et al. [30] proposed a method to predict ORC system performance based on the exploration and analysis of Support vector Machine (SVM) and BPNN. However, the above existing research related to ORC achieving prediction only focused the single working fluid or single ORC configuration, and the prediction scheme was relatively simple, so, the research content was not comprehensive enough.

Therefore, this paper established the thermodynamic model and the cycle database, which were based on BORC, RORC, IORC and CRIORC for seven working fluids including R141b, R236ea, R245fa, R245ca, R123, R114 and R11. After that, the best model parameters of BPNN and SVR were determined through error analysis, and the cycle database was used to train BPNN and SVR models to achieve the accurate prediction for the thermal efficiency and exergy efficiency of each ORC configuration for various working fluids. In addition, the reverse prediction for cycle parameters was also realized. Based on the above BPNN and SVR models, taking the RORC as an example, cycle parameter analysis and multi-objective optimization were implemented. Besides, a new approach based on Machine Learning models was used to achieve the relatively simple, quick and accurate optimization.

## 2. Research method

### 2.1. Methodology

Fig. 1 shows a general overview of the differences and connections between the research method in this paper and the traditional methods.

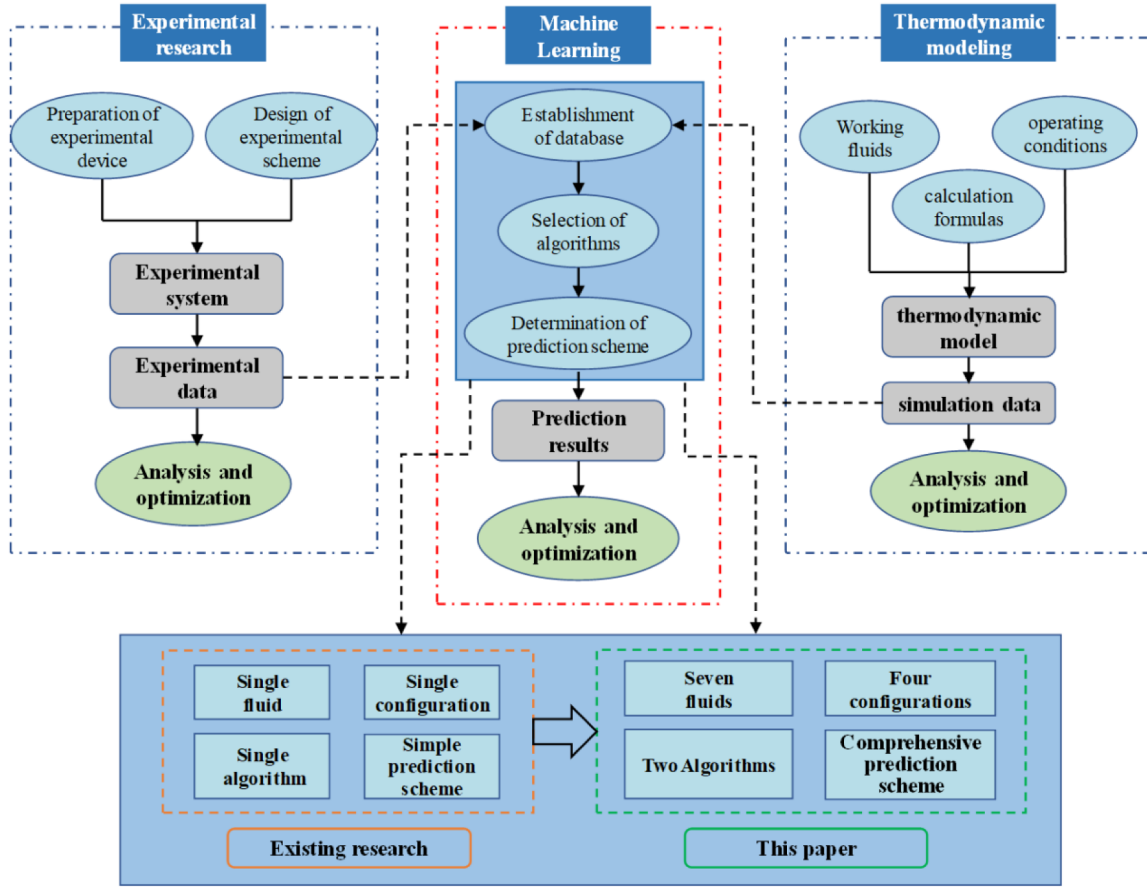


Fig. 1. The overview of research method.

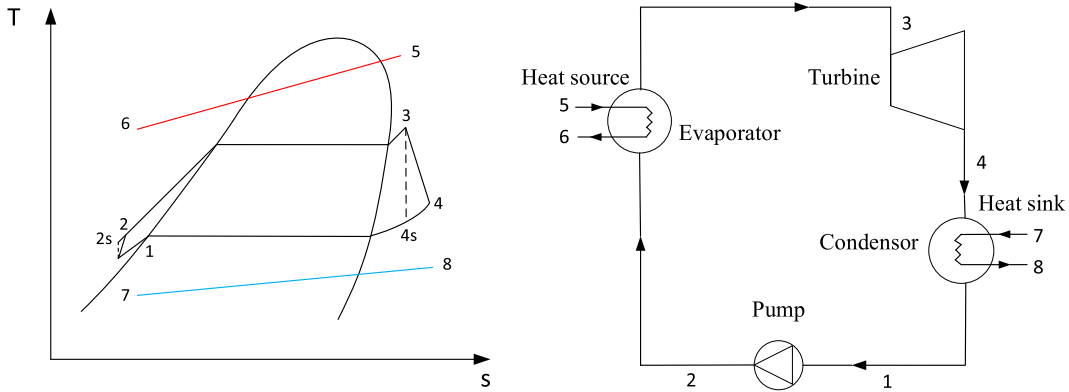


Fig. 2. BORC T-s diagram (left) and structure diagram (right).

First of all, the traditional methods including experimental research method and thermodynamic modeling method, and the method of this work is a Machine Learning method. The connects between them is that they have the same general workflow. They both obtain the results of performance data in someway and then analyze and optimize them. And the results of machine learning are predicted from experimental or simulated data. The differences between them is that both experimental or modeling methods need to calculate the performance results according to the traditional thermodynamics theory and equation, while machine learning is to obtain the performance results through prediction, and its internal operation has nothing to do with the

thermodynamics. One of the main purposes of this study is to explore the feasibility and effectiveness of this new method, so this study only chooses thermodynamic modeling for the moment rather than experiment as the data source of machine learning to avoid unnecessary costs. Through the work review in the introduction, it could roughly be summarized that the four deficiencies in the existing literature: single working fluid, single configuration, single algorithm and simple prediction scheme. In view of these deficiencies, the corresponding improvements in this study were made: seven working fluid, four configurations, two algorithms and the comprehensive prediction scheme. Working fluids and configurations, algorithms, and prediction scheme

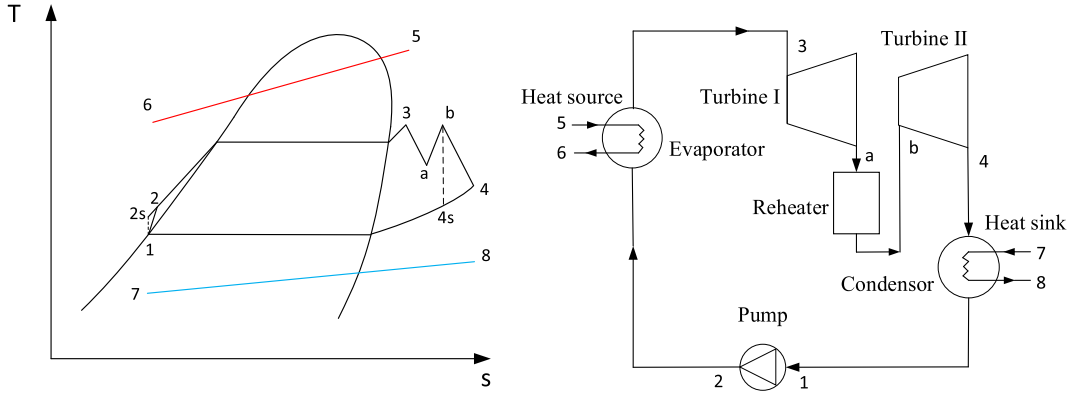


Fig. 3. RORC T-s diagram (left) and structure diagram (right).

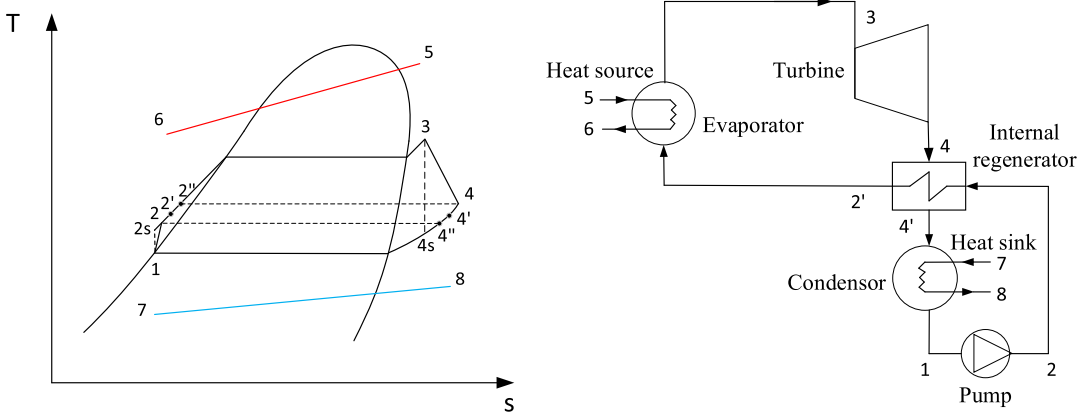


Fig. 4. IORC T-s diagram (left) and structure diagram (right).

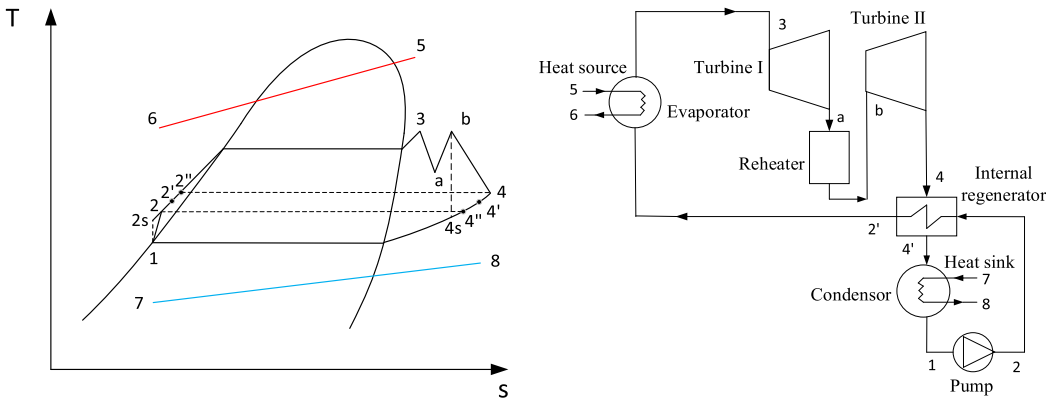


Fig. 5. CRIORC T-s diagram (left) and structure diagram (right).

are described in detail in 2.2, 2.3 and 3 section, respectively.

## 2.2. System description

This section mainly describes the working principles of basic organic Rankine cycle (BORC), reheating organic Rankine cycle (RORC), internal regenerative organic Rankine cycle (IORC), and combined reheating-internal regenerative organic Rankine cycle (CRIORC), and the thermodynamic models of them are established. All the four ORC

systems are subcritical ORC systems. In addition, there is the selection of working fluids.

### 2.2.1. Theoretical principles

The T-s diagrams (horizontal axis shows the temperature and vertical axis shows the entropy) and system structure diagrams of BORC, RORC, IORC and CRIORC are shown in Figs. 2–5 respectively.

For BORC, as shown in Fig. 2, the heat source fluid releases heat in the evaporator, heating the working fluid from state 2 to state 3 at

**Table 1**  
Thermophysical properties of working fluids.

Working fluid	Critical temperature ( $T_c$ ) / K	Critical pressure ( $P_c$ ) / kPa	Normal boiling point ( $T_b$ ) / K	Molecular mass	ODP	GWP
R141b	477.50	4212.00	305.20	116.95	0.11	630
R236ea	412.44	3501.98	279.34	152.04	0	1200
R245fa	427.16	3651.00	288.29	134.05	0	820
R245ca	447.57	3925.00	298.28	134.05	0	693
R123	456.83	3661.80	300.97	152.93	0.02	93
R114	418.83	3257.00	276.74	170.92	1	10,000
R11	385.12	4136.10	243.40	120.91	1	4600

**Table 2**  
Calculation conditions of ORC model.

Parameters	Values
Heat source temperature ( $T_h$ ) / K	400–480
Evaporating pressure ( $P_{eva}$ ) / kPa	500–3500
Condensing temperature ( $T_{con}$ ) / K	308.15–318.15
Degree of superheat ( $T_{sh}$ ) / K	0–21
Degree of supercooling ( $T_{sc}$ ) / K	0–11
Pinch point temperature in the evaporator ( $\Delta T_{ppe}$ ) / K	5–20
Reheating pressure ratio ( $\lambda$ )	0.1–0.6
Internal regenerator efficiency ( $\eta_{ir}$ )	0.65–0.9
Mass flow rate of heat source ( $m_t$ ) / kg/s	15
Heat sink temperature ( $T_s$ ) / K	293.15
Pinch point temperature in the condenser ( $\Delta T_{ppc}$ ) / K	3
Pump efficiency ( $\eta_p$ )	0.8
Turbine efficiency ( $\eta_t$ )	0.8
Atmospheric temperature ( $T_0$ ) / K	293.15
Atmospheric pressure ( $P_0$ ) / kPa	101.325

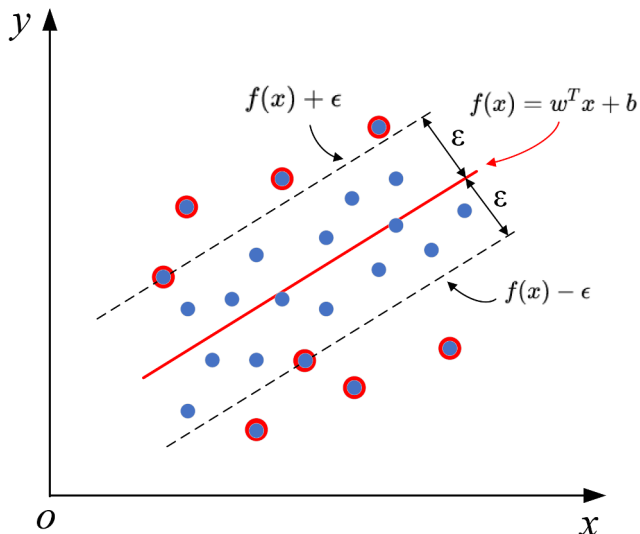


Fig. 6. The schematic diagram of the SVR.

constant pressure, and the vapor enters the turbine for the output of work, which is exhausted from state 4. After condensing to state 1 in the condenser, working fluid is compressed to high pressure state 2 by a pump. Afterwards, it is transported to the evaporator for an endothermic process. One cycle is completed as described above. The process 1–2 is the ideal compression process in the working fluid pump in  $T$ - $s$  diagram of Fig. 2. The process 3–4 is the ideal expansion process in the turbine in  $T$ - $s$  diagram of Fig. 2. Under the same initial

temperature (state 3) and backpressure (state 4), increasing the evaporating pressure means the increase of evaporating temperature, which increases the average temperature difference of the cycle (the increase of heat source temperature has the same effect). According to Carnot theorem, this will improve the thermal efficiency of the cycle. In addition, the increase of evaporating temperature increases the average endothermic temperature and reduces the heat transfer temperature difference (the decrease of heat source temperature could lead to the same result) in the evaporator, reducing the irreversible loss and improves the exergy efficiency. However, the increase of evaporating pressure will lead to the rapid reduction of exhaust steam dryness, which will badly affect the working process and life of the turbine.

For RORC, as shown in Fig. 3, after becoming vapor in evaporator, working fluid is transported into turbine I first to work, and then enters the reheater to be reheated, which will subsequently enter into turbine II to work again. And it is should be known that the efficiencies of turbine I and II are equal. After that, the cycle is completed through the condenser and the working fluid pump. With the addition of a heater (reheater) and a turbine, the work per kilogram of working fluid increases (do work twice). However, compared with BORC, the thermal and exergy efficiency of RORC cannot be directly judged, which depends on the level of reheating pressure (state a). However, it is important to know that the improvement of efficiency is not the fundamental purpose of reheating. The purpose is to avoid the adverse effects of increasing evaporation pressure on turbine life, which is especially important for some power generation devices that utilize saturated and micro-superheated steam. Therefore, when selecting the reheating pressure, the exhaust steam dryness must be made within the allowable range, and the reheating pressure must not blindly be increased in order to improve the efficiency performance. In addition, due to the increase of pipelines, valves and equipment, investment costs increase and cycle management is more complex.

For IORC, as shown in Fig. 4, before the working fluid compressed in the pump is transported to the evaporator, working fluid will conduct heat exchange process with exhaust steam from turbine in the internal regenerator. On the one hand, working fluid will be heated to state 2', and the corresponding ideal state is 2'' whose temperature equals to state 4 which is the outlet of the turbine II; on the other hand, the exhaust steam will be cooled to state 4', and the corresponding ideal state is 4'' whose temperature equals to state 2 which is the outlet of the working fluid pump. These ideal states are limited by the second law of thermodynamics. After that, the working fluid passes through the evaporator and the expander in turn, and the exhaust steam passes through the condenser and the pump in turn, and then both of them conduct heat exchange process in the internal regenerator again to complete the cycle. Internal regenerative process can reduce the heat transfer temperature difference of evaporator and condenser, so as to reduce the irreversible loss and improve exergy efficiency. Meanwhile, it can increase the average endothermic temperature and cycle average temperature difference to improve the thermal efficiency. Similarly, due to the increase of pipelines, valves and equipment, investment costs increase and cycle management is more complex.

For CRIORC, as shown in Fig. 5, the cycle processes of RORC and IORC are combined, and each process is same as the above. It should be known that the state 2'' and 4'' are the corresponding ideal state of 2' and 4' respectively as the same as IORC of Fig. 4. Based on the above thermodynamic analysis of BORC, RORC and IORC, it is necessary to combine RORC and IORC to observe its cycle performance. It could be reasonably inferred that CRIORC's thermal efficiency and exergy efficiency will be greatly improved under appropriate operating parameters and conditions.

In order to simplify the model of each ORC configuration, some general assumptions are taken into account:

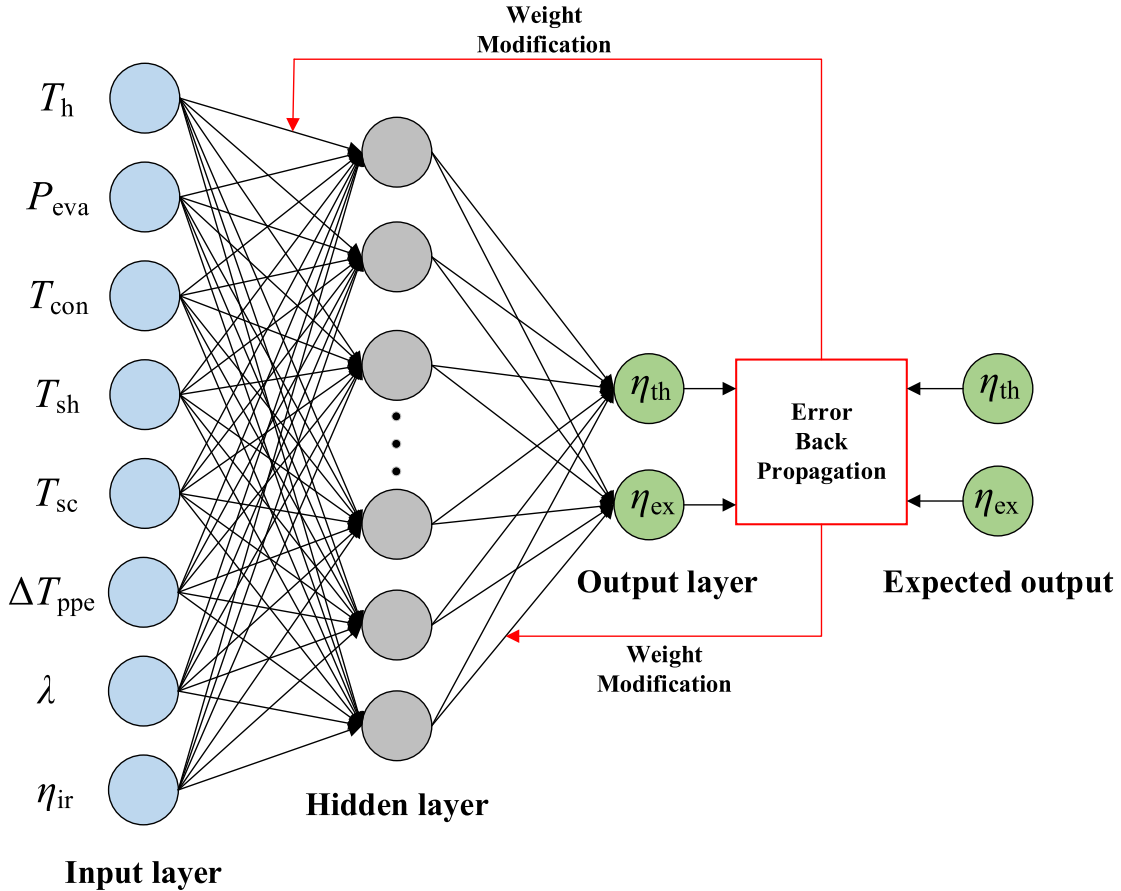


Fig. 7. The schematic diagram of the BPNN.

**Table 3**

Prediction error by SVR using different kernel functions.

Kernel function	$\eta_{th}$			$\eta_{ex}$				$R^2$
	MSE /*10 <sup>-4</sup>	MAE	MRE /%	R <sup>2</sup>	MSE /*10 <sup>-4</sup>	MAE	MRE /%	
RBF	0.0207	0.0013	1.0436	0.9975	0.2456	0.0041	1.0798	0.9948
poly	0.0225	0.0014	1.1263	0.9934	0.6857	0.0060	1.5094	0.9834
linear	1.0087	0.0075	6.5656	0.8775	9.2497	0.0234	6.9534	0.8054

- 1) The system is in steady state.
- 2) The pressure drop and heat loss of all heat exchangers and pipelines are negligible.
- 3) The kinetic energy and potential energy of the system are ignored.
- 4) The condenser outlet is saturated liquid state except for BORC.

### 2.2.2. Working fluid selection

Considering the subcritical ORC characteristics and heat source temperature and according to the commonly used working fluids in the existing literature, seven working fluids including R141b, R236ea, R245fa, R245ca, R123, R114 and R11 were selected as the research objects. The main parameters of them are shown in Table 1.

### 2.2.3. Thermodynamic modeling

The above BORC, RORC, IORC and CRIORC configurations are mainly composed of evaporator, turbine, condenser, working fluid pump, reheat and internal regenerator. The system structure diagram and *T-s* diagram are shown in Figs. 2 to 5. The energy analysis of each

part is as below.

- 1) For the evaporator:

BORC, RORC:

$$Q_{eva} = m_f (H_3 - H_2) \quad (1)$$

IORC, CRIORC:

$$Q_{eva} = m_f (H_3 - H_2) \quad (2)$$

- 2) For the turbine:

BORC, IORC:

$$W_{tur} = m_f (H_3 - H_{4s}) \eta_t \quad (3)$$

RORC, CRIORC:

$$W_{turI} = m_f (H_3 - H_{as}) \eta_t \quad (4)$$

$$W_{turII} = m_f (H_b - H_{4s}) \eta_t \quad (5)$$

- 3) For the condenser:

BORC, RORC:

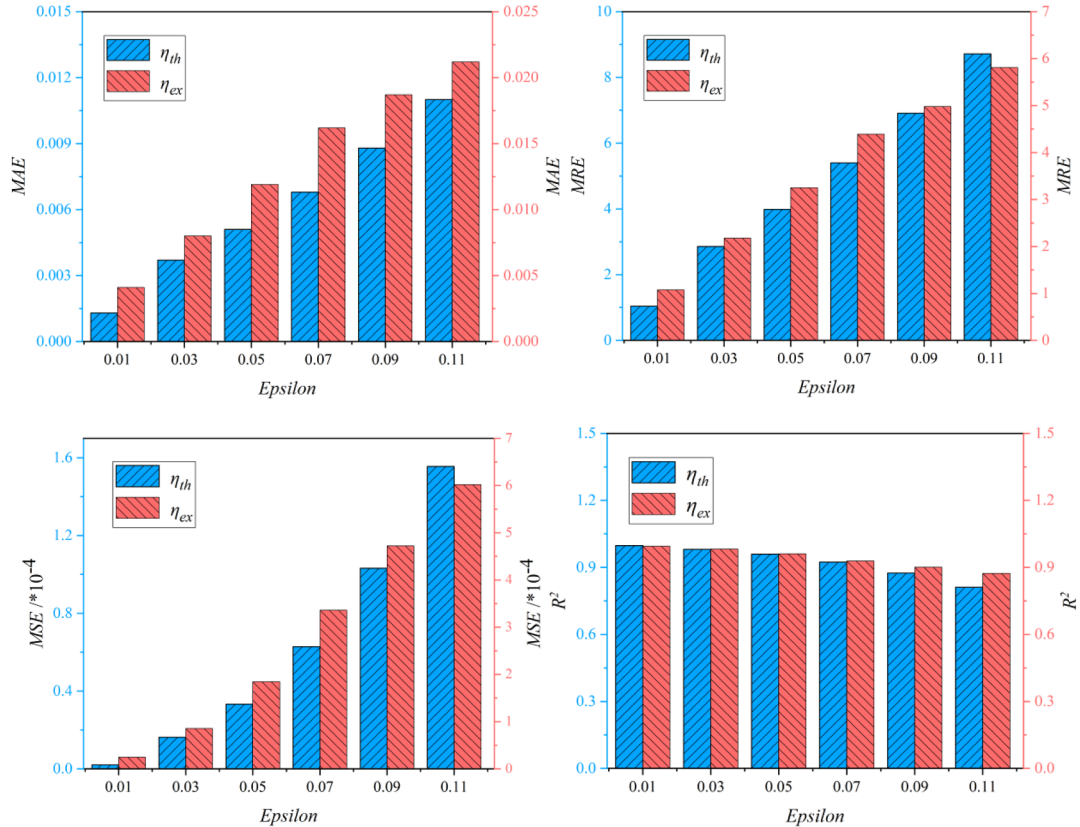


Fig. 8. The effect of epsilon on the SVR prediction performance.

**Table 4**

Prediction error by SVR with different epsilon value.

$\eta_{th}$				$\eta_{ex}$				
epsilon	MSE $/\times 10^{-4}$	MAE	MRE/%	$R^2$	MSE $/\times 10^{-4}$	MAE	MRE/%	$R^2$
0.01	0.0207	0.0013	1.0436	0.9975	0.2456	0.0041	1.0798	0.9948
0.03	0.0163	0.0037	2.8578	0.9803	0.8571	0.0080	2.1793	0.9820
0.05	0.3333	0.0051	3.9897	0.9595	1.84 40	0.0119	3.2503	0.9612
0.07	0.6282	0.0068	5.4028	0.9237	3.3631	0.0162	4.3893	0.9292
0.09	1.0324	0.0088	6.9126	0.8746	4.7219	0.0187	4.9821	0.9007
0.11	1.5560	0.0110	8.7148	0.8110	6.0217	0.0212	5.8101	0.8733

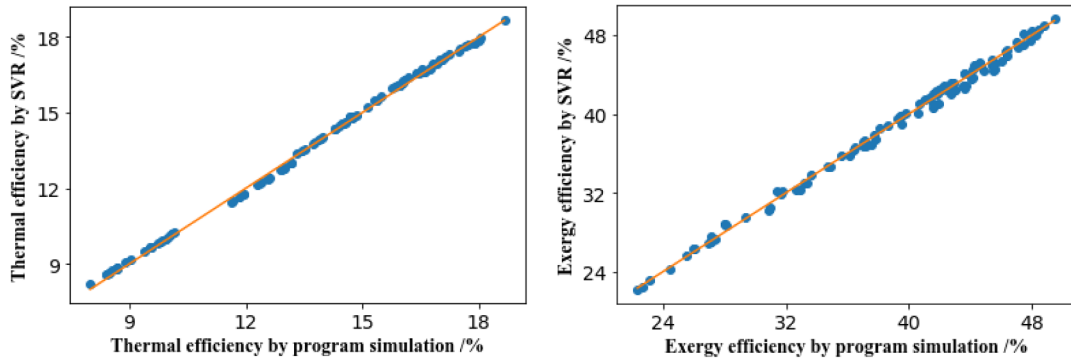


Fig. 9. Prediction result by SVR with rbf kernel function and epsilon to be 0.01.

$$Q_{\text{con}} = m_f (H_4 - H_1) \quad (6)$$

IORC, CRIORC:

$$Q_{\text{con}} = m_f (H_4' - H_1) \quad (7)$$

4) For the pump:

BORC, RORC, IORC, CRIORC:

$$W_{\text{pump}} = m_f (H_{2s} - H_1) / \eta_p \quad (8)$$

5) For the reheater:

RORC, CRIORC:

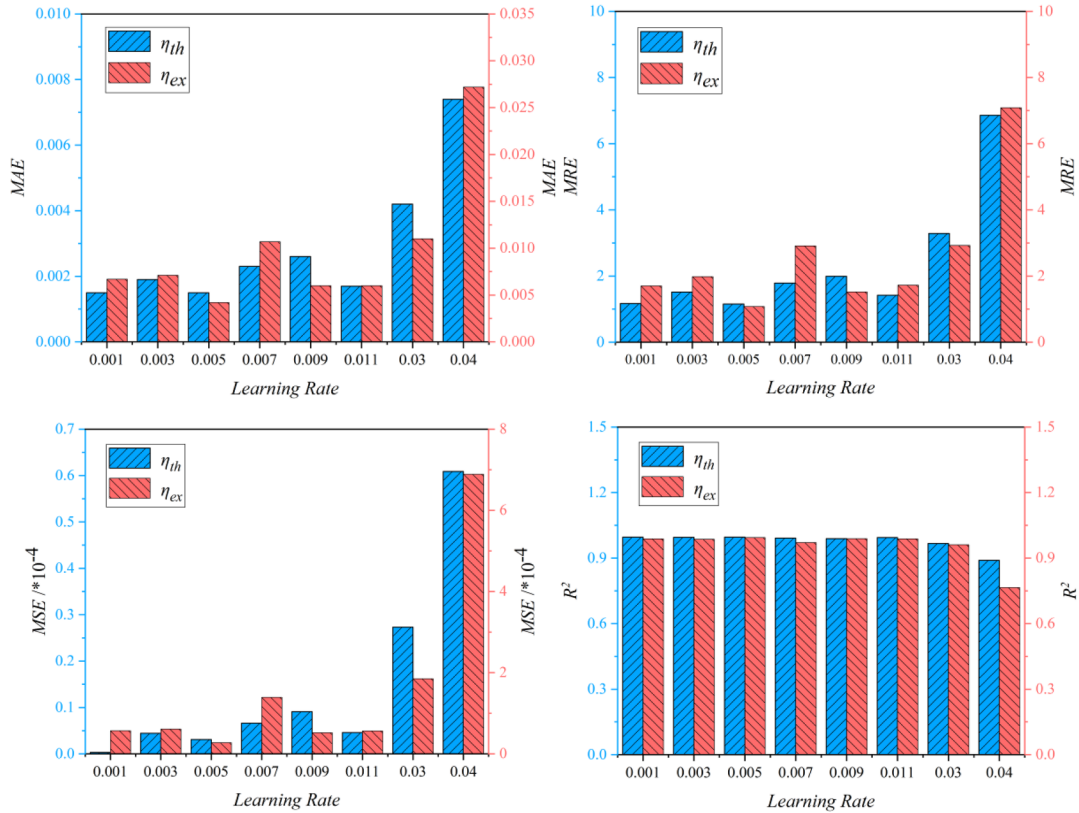


Fig. 10. The effect of learning rate on the BPNN prediction performance.

**Table 5**

Prediction error by BPNN with different learning rate value.

LearningRate	$\eta_{th}$				$\eta_{ex}$			
	MSE /*10 <sup>-4</sup>	MAE	MRE/%	R <sup>2</sup>	MSE /*10 <sup>-4</sup>	MAE	MRE /%	R <sup>2</sup>
0.001	0.0305	0.0016	1.1701	0.9963	0.5714	0.0067	1.7015	0.9880
0.003	0.0446	0.0019	1.5152	0.9946	0.6134	0.0071	1.9818	0.9871
0.005	0.0311	0.0015	1.1550	0.9962	0.2760	0.0042	1.0786	0.9942
0.007	0.0662	0.0023	1.7867	0.9920	1.3964	0.0107	2.9108	0.9706
0.009	0.0910	0.0026	1.9898	0.9889	0.5194	0.0060	1.5210	0.9891
0.011	0.0458	0.0017	1.4198	0.9944	0.5661	0.0060	1.7243	0.9881
0.03	0.2733	0.0042	3.2839	0.9668	1.8496	0.0110	2.9261	0.9611
0.04	1.2392	0.0094	7.8579	0.8495	0.0017	0.0322	9.0844	0.6446

$$Q_r = m_f (H_b - H_a) \quad (9)$$

6) For the regenerator:  
IORC, CRIORC:

$$\eta_{ir} = \frac{(H_4 - H_4')}{(H_4 - H_{4''})} = \frac{(H_2 - H_{2'})}{(H_2 - H_{2''})} \quad (10)$$

$$T_{4'} = T_2 \quad (11)$$

$$T_{2'} = T_4 \quad (12)$$

$$m_f (H_4 - H_4') = m_f (H_{2'} - H_2) \quad (13)$$

Based on the above energy analysis for each component, the thermal and exergy efficiencies of cycle are calculated as follows:

1) For the thermal efficiency of cycle:

Net power output:

BORC, IORC:

$$W_{net} = W_{tur} - W_{pump} \quad (14)$$

RORC, CRIORC:

$$W_{net} = W_{tur\ I} + W_{tur\ II} - W_{pump} \quad (15)$$

Thermal efficiency:  
BORC, IORC:

$$\eta_{th} = W_{net}/Q_{eva} \quad (16)$$

RORC, CRIORC:

$$\eta_{th} = W_{net}/(Q_{eva} + Q_r) \quad (17)$$

2) For the exergy efficiency of cycle:

The exergy supplied by the heat source:

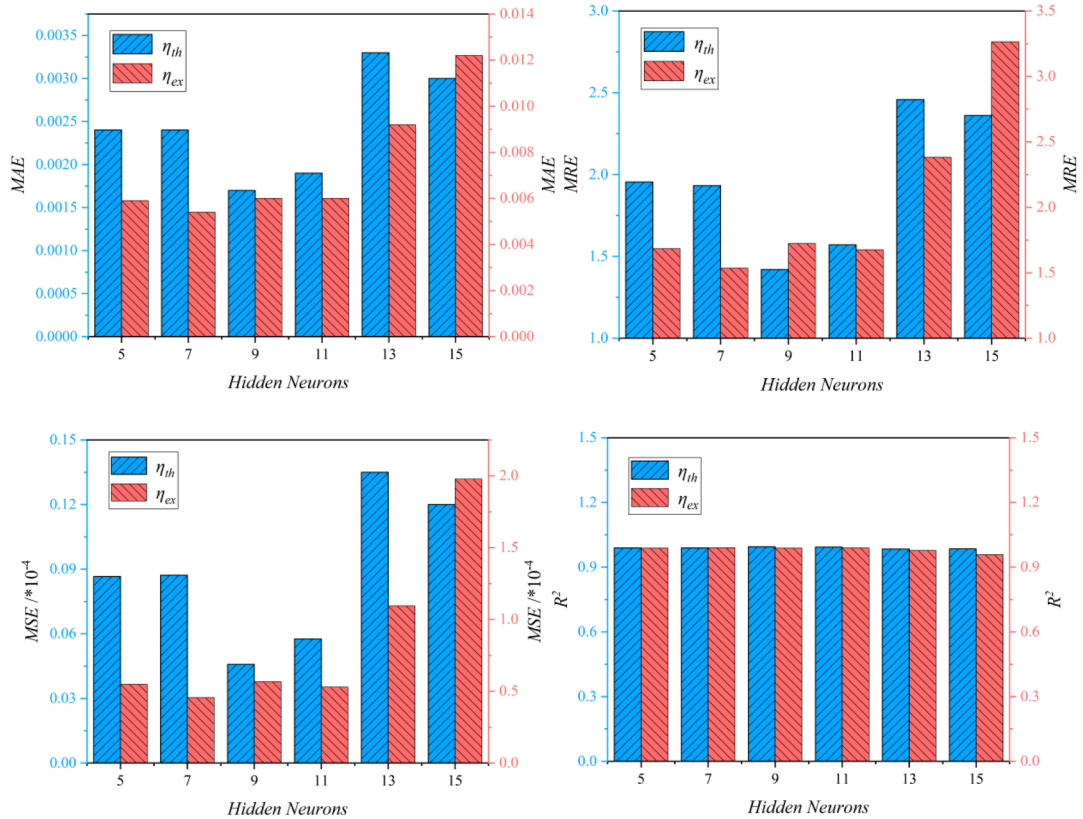


Fig. 11. The effect of hidden neurons on the BPNN prediction performance.

Table 6

Prediction error by BPNN with different hidden neurons value.

Hidden neurons	$\eta_{th}$				$\eta_{ex}$			
	MSE/*10 <sup>-4</sup>	MAE	MRE/%	R <sup>2</sup>	MSE/*10 <sup>-4</sup>	MAE	MRE/%	R <sup>2</sup>
5	0.0866	0.0024	1.9555	0.9895	0.5495	0.0059	1.6842	0.9884
7	0.0872	0.0024	1.9318	0.9894	0.4560	0.0054	1.5361	0.9904
9	0.0458	0.0017	1.4198	0.9944	0.5661	0.0060	1.7243	0.9881
11	0.0576	0.0019	1.5709	0.9930	0.5301	0.0060	1.6759	0.9888
13	0.1349	0.0033	2.4583	0.9836	1.0949	0.0092	2.3832	0.9770
15	0.1201	0.0030	2.3612	0.9854	1.9778	0.0123	3.2648	0.9584

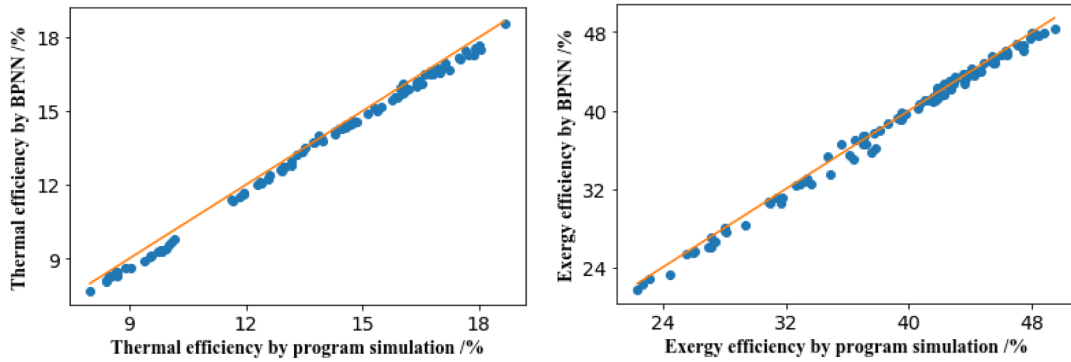


Fig. 12. Prediction result by BPNN with learning rate and hidden neurons to be 0.05 and 9 respectively.

BORC, IORC:

$$E = \left(1 - \frac{T_0}{T_h}\right)Q_{eva} \quad (18)$$

RORC, CRIORC:

$$E = \left(1 - \frac{T_0}{T_h}\right)(Q_{eva} + Q_r) \quad (19)$$

Exergy efficiency:

$$\eta_{ex} = \frac{W_{net}}{E} \quad (20)$$

**Table 7**

Input value of prediction model for four ORC configurations.

	$T_h$	$P_{eva}$	$T_{con}$	$T_{sh}$	$T_{sc}$	$\Delta T_{ppe}$	$\lambda$	$\eta_{ir}$
BORC	✓	✓		✓	✓	✓		
RORC	✓	✓		✓		✓	✓	
IORC	✓	✓		✓		✓		✓
CRIORC	✓	✓		✓		✓		✓

In these models, the hot air under atmospheric pressure is taken as the heat source, and the mass flow rate is 15 kg/s. The normal temperature water is the heat sink, and the mass flow rate is calculated to meet the cooling requirements. Variable calculation conditions are heat source temperature, evaporating pressure, condensing temperature, the degree of superheat, the degree of supercooling, pinch point temperature in the evaporator, reheat pressure ratio and regenerator efficiency, etc. (the degree of supercooling of RORC, IORC and CRIORC is fixed at 0 K, and the condensing temperature of CRIORC is fixed at 308.15 k) The fixed calculation conditions are mass flow rate of heat source, temperature of heat sink, pinch point temperature in the condenser, isentropic efficiency of working fluid pump and turbine, atmospheric temperature and pressure, etc. These calculation conditions of the ORC models are listed in Table 2. The cycle dataset is generated by taking values of variable calculation parameters at certain intervals. Specifically, the intervals of heat source temperature, evaporating pressure, condensing temperature, degree of superheat, degree of supercooling, pinch point temperature in the evaporator, reheating pressure ratio and internal regenerator efficiency are 10 K, 500 kPa, 2 K, 4 K, 2 K, 2 K, 0.1, 0.05 respectively.

In this study, ORC simulation code is developed with python language, and parameters of state points of each working fluid are calculated based on REFPROP version 9.1.

### 2.3. Algorithm selection

Actually, the pre-screening of algorithms was carried out in the preliminary work. ORC's performance prediction errors of Decision Tree, Random Forest and Support Vector regression (SVR) algorithms were compared, and the results showed that SVR had the best performance. In addition, Back Propagation Neural Network (BPNN) algorithm has been considered as one of the most widely used and mature artificial neural network algorithms. Therefore, BPNN and SVR algorithm were selected for research in this paper.

**Table 8**

Prediction error for thermal efficiency.

Model	WorkingFluid	BORC		RORC		IORC		CRIORC	
		MRE/%	$R^2$	MRE/%	$R^2$	MRE/%	$R^2$	MRE/%	$R^2$
BPNN	R141b	1.5470	0.9947	3.0272	0.9794	2.4001	0.9915	0.6651	0.9980
	R236ea	4.5287	0.9852	3.8182	0.9585	3.2059	0.9882	1.1501	0.9940
	R245fa	2.1792	0.9922	2.2802	0.9859	3.5453	0.9812	1.1932	0.9957
	R245ca	0.9760	0.9978	2.3175	0.9840	3.3212	0.9750	0.8500	0.9975
	R123	2.7315	0.9848	2.1772	0.9888	4.4211	0.9689	0.7446	0.9988
	R114	2.2486	0.9965	1.7362	0.9858	3.9879	0.9819	2.1952	0.9836
	R11	3.9372	0.9801	3.8571	0.9663	2.8318	0.9896	0.4949	0.9992
SVR	R141b	0.9187	0.9981	1.1143	0.9973	1.2631	0.9981	1.0227	0.9964
	R236ea	2.1730	0.9982	0.7900	0.9962	1.4137	0.9978	0.6932	0.9983
	R245fa	1.4734	0.9979	1.0172	0.9972	1.4185	0.9980	0.9251	0.9977
	R245ca	1.1253	0.9977	0.8672	0.9975	1.1383	0.9978	0.9602	0.9977
	R123	1.1448	0.9979	1.0745	0.9973	1.1561	0.9980	1.2110	0.9976
	R114	1.7235	0.9983	0.6811	0.9977	1.5187	0.9984	0.8913	0.9960
	R11	1.1902	0.9980	0.9619	0.9976	1.2722	0.9981	1.0516	0.9974

### 2.3.1. Support Vector regression (SVR)

SVR, derived from the Support Vector Machine (SVM) algorithm, is an algorithm that applies SVM to regression problems. Fig. 6 shows the schematic diagram of the SVR that could show the fundamental operational principle of SVR. For the ordinary linear regression model, it takes the distance from the actual position of all samples to the linear function as the loss and obtains the parameters of the linear function by minimizing the loss function. For linear regression, a sample that does not fall exactly on the linear function of the model will be included in loss. However, SVR creates an “interval band” on both sides of the linear function (Eq.21) as shown in Fig. 6, and does not calculate the loss for all samples falling into the interval band. Only those outside or on the edge of the interval band are included in the loss function (Eq. 22). The model is then optimized by minimizing the width of the interval band and the total loss. In this way, only those samples circled in red as shown in Fig. 6 (either outside or on the edge of the interval band) are included in final total loss. In conclusion, key parameters of SVR algorithm [31] mainly include kernel function, epsilon (i.e.,  $\epsilon$ ), gamma, C, etc. Different values of these parameters will affect the prediction accuracy. In section 4 of this paper, the appropriate parameter values will be explored for kernel function and epsilon which have a larger impact.

$$f(x) = w^T x + b \quad (21)$$

$$\text{Loss} = \frac{1}{2} \|w\|^2 + C \sum_{i=1}^m l_\epsilon(f(x_i), y_i) \quad (22)$$

$$l_\epsilon(z) = \begin{cases} 0, & \text{if } |z| \leq \epsilon \\ |z| - \epsilon & \text{otherwise} \end{cases} \quad (23)$$

Eq. (21) is the SVR model function which is the red line in Fig. 6, and w and b are two model parameters to be solved, and x is the input sample. Eq. (22) is the loss function. By minimizing the loss function, w and b will be determined, and then model function will be obtained. In addition,  $l_\epsilon(z)$  is called as  $\epsilon$ -insensitive loss function which is calculated as Eq. (23), and z is the distance from each sample to the f(x) (i.e., the red line in Fig. 6)

### 2.3.2. Back Propagation Neural Network (BPNN)

BPNN [32] is considered as one of the most widely used and mature artificial neural networks. It is a multi-layer feedforward neural network with error back-propagation learning algorithm as shown in Fig. 7. It is composed of input layer, hidden layer and output layer. The input layer consists of the variables including  $T_h$ ,  $P_{eva}$ ,  $T_{con}$ ,  $T_{sh}$ ,  $T_{sc}$ ,

**Table 9**

Prediction error for exergy efficiency.

Model	WorkingFluid	BORC	RORC	IORC	CRIORC
BPNN	R141b	MRE /%	R <sup>2</sup>	MRE /%	R <sup>2</sup>
	R236ea	2.2808	0.9706	3.2345	0.9673
	R245fa	3.7989	0.9861	4.0901	0.9509
	R245ca	1.9909	0.9933	3.5480	0.9711
	R123	1.7828	0.9906	4.5813	0.9237
	R114	2.8199	0.9784	4.8777	0.9387
SVR	R11	1.1990	0.9942	4.3102	0.9430
	R141b	2.8085	0.9731	2.6052	0.9752
	R236ea	3.9239	0.9731	2.6052	0.9752
	R245fa	1.0120	0.9956	1.1784	0.9942
	R245ca	2.2658	0.9969	1.0361	0.9926
	R123	1.7987	0.9947	1.1504	0.9957
SVR	R114	1.2655	0.9957	1.0622	0.9946
	R11	1.3424	0.9952	1.0781	0.9959
	R11	1.6052	0.9978	0.7471	0.9970
	R11	1.5416	0.9935	1.1503	0.9936
	R11				1.3363
	R11				0.9957

$\Delta T_{\text{ppe}}$ ,  $\lambda$ ,  $\eta_{\text{ir}}$ . The nodes in hidden layer accept the values (Eq. (24)) from input layer and perform nonlinear processing (Eq. (25)). The results of the hidden layer are finally delivered to the output layer. The process mentioned above is called “feed forward connection”. Then the errors between the output values ( $\eta_{\text{th}}$  and  $\eta_{\text{ex}}$ ) and expected values will be calculated by Eq. (26). If the errors are beyond the specified interval, the error propagation process will be performed to modify the weight of the neural network. This process is called as “error feedback connection”. The key parameters of BPNN algorithm mainly include learning rate, number of hidden layers, number of hidden neurons, etc. In section 4, this paper will explore appropriate parameter values for the learning rate and the number of hidden neurons that have a larger impact.

$$Z = \sum_{i=1}^M (w_{ij}x_i + b_j) \quad (24)$$

$$f(Z) = \frac{1}{1 + e^{-Z}} \quad (25)$$

$$E = \frac{1}{2} \sum_i^I (y_i - \hat{y}_i)^2 \quad (26)$$

In Eq. (24), Z denotes the output value of the input layer, and M denotes the number of the input variables, and  $x_i$  denotes i<sup>th</sup> sample. The  $w_{ij}$  is the link weight of the i<sup>th</sup> input value to the j<sup>th</sup> hidden layer node and  $b_j$  is the threshold value of the j<sup>th</sup> node in hidden layer. Eq. (25) is called as the activation function. Eq. (26) is the error function. I stands for the dimensions of the output value which is two dimensions in this paper. The  $y_i$  and  $\hat{y}_i$  denote the output value and the expected value, respectively.

### 2.3.3. Error evaluation index

In order to evaluate the prediction results of the two algorithm models, mean squared error (MSE), mean absolute error (MAE), mean relative error (MRE) and determination coefficient R<sup>2</sup> are adopted in this paper. In general, as RMSE and MAE are smaller, the prediction results are more accurate. But different cases usually cause they have different magnitudes, such as prediction for house prices and people height. So, the readability of these two indices is not good. MRE and R<sup>2</sup> have good readability. MRE is a percentage, and the smaller it is, the smaller the mean relative error of the prediction will be. The range of R<sup>2</sup> is 0 to 1, and the closer to 1, the higher the accuracy of the prediction is, and the closer to 0, the lower the accuracy is. The specific formulas of the above four evaluation indices are defined as below.

$$\text{MSE} = \frac{1}{m} \sum_{i=1}^m (y_i - \hat{y}_i)^2 \quad (27)$$

$$\text{MAE} = \frac{1}{m} \sum_{i=1}^m |(y_i - \hat{y}_i)| \quad (28)$$

$$\text{MRE} = \frac{1}{m} \sum_{i=1}^m \frac{|(y_i - \hat{y}_i)|}{y_i} \times 100\% \quad (29)$$

$$R^2 = 1 - \frac{\sum_i^I (\hat{y}_i - y_i)^2}{\sum_i^I (\bar{y}_i - y_i)^2} \quad (30)$$

## 3. Prediction result and discussion

### 3.1. Parameters determination for SVR and BPNN

In order to determine the appropriate parameters value of SVR and BPNN, taking the cycle data of BORC model using R141b for test, the input values are evaporating pressure, heat source temperature, condensing temperature, degree of superheat, degree of supercooling and pinch point temperature in the evaporator, and the output values are thermal efficiency and exergy efficiency. In its database, 40,000 groups of data(BORC using R141b) are randomly selected as the training set, and 100 groups of data(BORC using R141b) are the test set to conduct the error analysis of the prediction results. The specific method is as follows.

#### 3.1.1. Determination for kernel function and epsilon of SVR

The common kernel functions of SVR include radial basis function (RBF), linear function and poly functions. Epsilon has a default value of 0.1, which is set between 0.01 and 0.11 in this study. For the three kernel functions (epsilon = 0.01), the prediction errors of thermal efficiency and exergy efficiency are shown in Table 3. It could be seen that the SVR model with RBF kernel function is the best, so this paper chooses RBF kernel function. According to the SVR model with RBF kernel function, different values of epsilon were taken to obtain the corresponding prediction results of thermal and exergy efficiency which are shown in Fig. 8, and the specific error values are listed in Table 4. It could be seen from the figure, the MAE, MRE and MSE of prediction results of thermal and exergy efficiency decrease with the decrease of epsilon, and the change is relatively obvious. R<sup>2</sup> increases with the decrease of epsilon, but not too much. When epsilon is set to be 0.01,

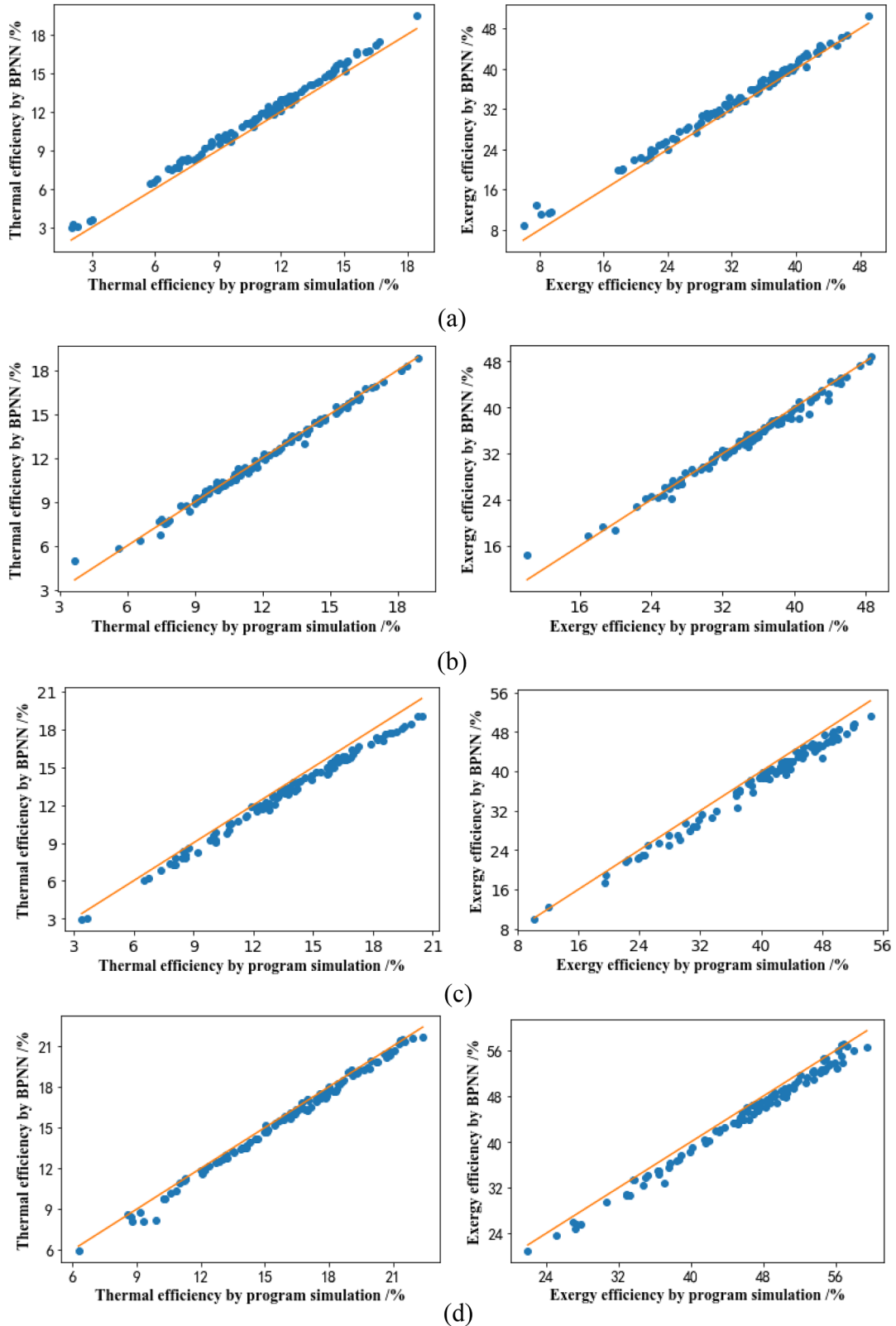


Fig. 13. Prediction result by BPNN for thermal(left) and exergy(right) efficiency of BORC(a), RORC(b), IORC(c), CRIORC(d).

the prediction error of SVR is the smallest. It should be noted that when epsilon continues to take the value smaller than 0.01, the prediction error of the SVR will continue to decrease, but the change is very small and the training time increases significantly. Therefore, it is more appropriate to choose 0.01 for epsilon.

Therefore, in this study, the kernel function of the SVR model is RBF kernel function, epsilon value is 0.01. And its prediction results of thermal efficiency and exergy efficiency of BORC using R141b are shown in Fig. 9.

**Table 10**

Prediction error with input value of working fluid number.

Model	Output	BORC		RORC		IORC		CRIORC	$R^2$
		MRE/%	$R^2$	MRE/%	$R^2$	MRE/%	$R^2$		
BPNN	$\eta_{th}$	5.1619	0.9797	3.2812	0.9803	4.3633	0.9725	2.1940	0.9896
	$\eta_{ex}$	5.9989	0.9674	5.2393	0.9332	2.5274	0.9857	2.6858	0.9766
SVR	$\eta_{th}$	20.4556	0.7292	13.3048	0.7044	9.2761	0.8503	9.3223	0.8035
	$\eta_{ex}$	20.8007	0.6320	12.6315	0.5813	9.4634	0.7817	8.7280	0.7365

### 3.1.2. Determination for learning rate and hidden neurons of BPNN

The learning rate of BPNN is set between 0.001 and 0.04, the number of hidden neurons is set between 5 and 15. Besides, the number of hidden layers is set at 1; epochs is set at 100; batch size is set at 20.

Based on different values of the learning rate, the corresponding RMSE, MAE, MRE and R<sup>2</sup> of the prediction results of thermal and exergy efficiency are obtained which are shown in Fig. 10, and the specific error values were listed in Table 5.

It could be seen from figure that the MSE, MAE, MRE of prediction results fluctuate in a small range with the increase of learning rate when learning rate is between 0.001 and 0.011, and increase obviously after 0.011 of learning rate. The MSE, MAE, MRE will be minimum when the learning rate is 0.005. The R<sup>2</sup> remains basically unchanged with the increase of learning rate when the learning rate between 0.001 and 0.011, and decreased significantly after 0.011.

Based on different number of hidden neurons, the MSE, MAE, MRE, R<sup>2</sup> of prediction results for thermal efficiency and exergy efficiency are obtained which are shown in Fig. 11, and the specific error values are shown in Table 6.

It could be seen from the figure that with the increase of the hidden neurons, the MAE, MRE and MSE of the prediction results of thermal and exergy efficiency decrease first and then increase. And the R<sup>2</sup> remains basically unchanged with the increase of the hidden neurons. Based on the four evaluation indices, the prediction error is the smallest when the hidden neurons are 9.

Therefore, in this study, the learning rate of BPNN model is 0.05, and the number of hidden neurons is 9. Its prediction results of thermal efficiency and exergy efficiency of BORC using R141b are shown in Fig. 12.

Besides, the time of simulation and prediction for 40,000 groups of data of BORC with R141b was tested, and the results showed that the time of simulation, BPNN and SVR was 33.04, 1.67 and 4.64 s respectively. So, the speed of prediction of BPNN and SVR was about 20 and 7 times respectively as faster as simulation.

### 3.2. Prediction performance for $\eta_{th}$ and $\eta_{ex}$ of BORC, RORC, IORC and CRIORC

Based on the optimal parameters determined in Section 4.1, BPNN and SVR models were established to predict the thermal and exergy efficiency of BORC, RORC, IORC and CRIORC. 40,000 groups of data were randomly selected from each configuration as the training set and 100 groups of data were randomly selected from each configuration as the test set. The input values of each ORC configuration are listed in Table 7, and the output values are thermal efficiency and exergy efficiency.

#### 3.2.1. Individual prediction for each working fluid

Firstly, the prediction for each working fluid of four ORC configurations was conducted individually. The error values of the prediction results of thermal efficiency and exergy efficiency were listed respectively in Tables 8 and 9. In terms of readability, only MRE and R<sup>2</sup> values were listed here for intuitive comparison.

Taking the relatively intuitive MRE as example, it could be seen that for the prediction results of thermal efficiency and exergy efficiency, the MRE of BPNN basically kept in the range of 1%–5%, and the MRE of SVR basically kept in the range of 1%–2%. Therefore, both the prediction results of BPNN and SVR are relatively accurate, and the prediction error of SVR is relatively smaller. In conclusion, both of BPNN and SVR models could accurately predict the thermal efficiency and exergy efficiency of BORC, RORC, IORC and CRIORC with each working fluid.

#### 3.2.2. Combined prediction for seven working fluids

In 3.2.1, BPNN and SVR models made the individual prediction for each working fluid. In the following, seven working fluids will be gathered to achieve the combined prediction. The key point is to determine the input form of working fluid as a kind of input value.

**3.2.2.1. Working fluid number as the input value.** The first type of input form is relatively simple. Seven working fluids are numbered 1–7, and the corresponding number of each working fluid is taken as the input value for the working fluid. After training of BPNN and SVR models, the prediction results for the test set of two models were obtained.

The prediction results of the BPNN model are shown in Fig. 13. The specific error values are listed in Table 10. It could be seen that the prediction results of BPNN are still relatively accurate. Compared with the prediction results in 3.2.1, MRE slightly increases and basically remains between 3% and 5%.

The prediction results of the SVR model are shown in Fig. 14. The specific error value is listed in Table 10. It could be seen that the prediction results of SVR are very poor compared with the prediction results in 3.2.1. MRE basically remains between 8% and 20%, so the error value reaches the unacceptable range.

In order to solve the problem that the SVR model has a large error in the combined prediction for seven working fluids, another input form of working fluid was proposed in 3.2.2.2.

**3.2.2.2. Thermophysical properties of working fluid as the input value.** The second type of input form no longer takes the number of working fluids as the input value, but takes the thermophysical property parameters of working fluid as the input value, including the critical temperature, critical pressure and normal boiling point. It is more accurate to describe the characteristics of working fluid in the form of three thermophysical property parameters than the simple number. Moreover, thermophysical property parameters will directly affect the calculation process of ORC model, which have a greater correlation with the output value. Theoretically, it could be reasonably inferred that the accuracy of prediction would be improved.

The prediction results of BPNN are shown in Fig. 15, and the specific error values are listed in Table 11. It could be seen that the prediction results of BPNN are still relatively accurate and basically consistent with the prediction results with the number form as the input value.

The prediction results of SVR are shown in Fig. 16, and the specific error values are listed in Table 11. It could be seen that after using the

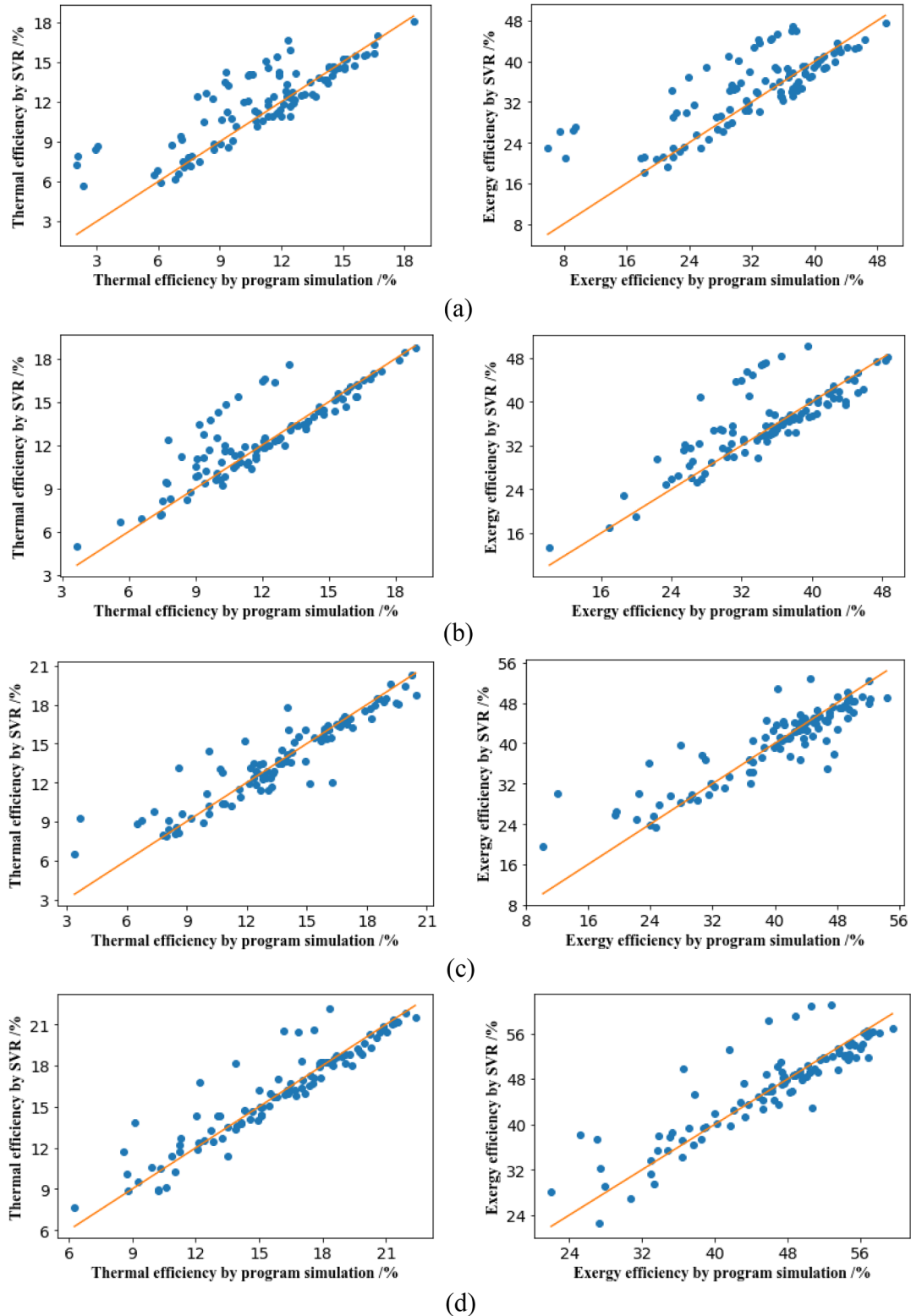
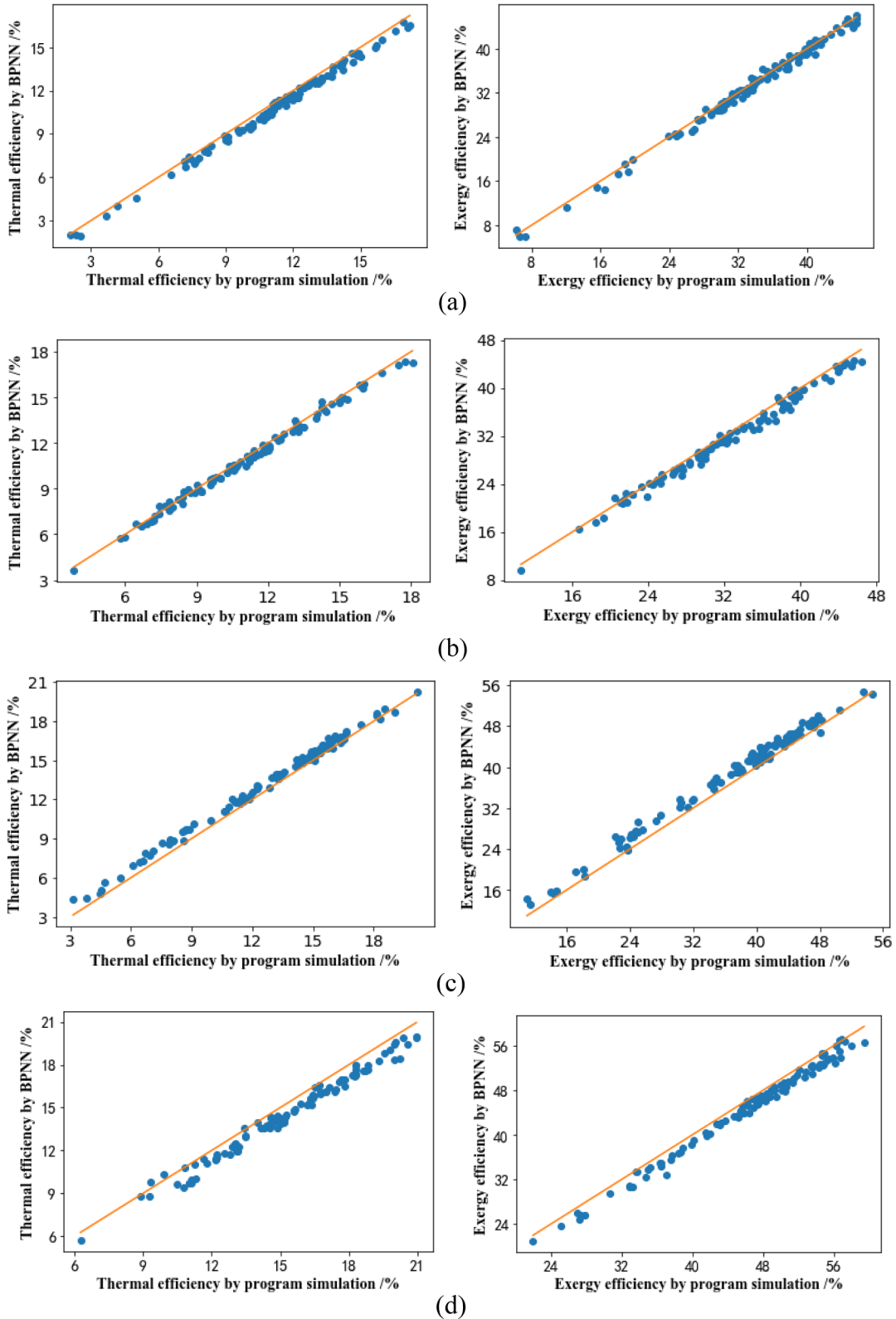


Fig. 14. Prediction result by SVR for thermal(left) and exergy(right) efficiency of BORC(a), RORC(b), IORC(c), CRIORC(d).

second input form of working fluid, the prediction results of SVR become accurate, and MRE basically remains between 1% and 3%. It is basically consistent with the prediction results of individual prediction for each working fluid in 3.2.1.

On the whole, BPNN maintained good prediction results in 3.2.1, 3.2.2.1 and 3.2.2.2, while SVR showed poor prediction results in 3.2.2.1. After changing the input form of working fluid, the prediction results were improved significantly, which are basically consistent with



**Fig. 15.** Prediction result by BPNN for thermal(left) and exergy(right) efficiency of BORC(a), RORC(b), IORC(c), CRIORC(d).

the prediction accuracy in 3.2.1. To some extent, the reason for this result lies in the different internal operation mechanism of the two algorithms and the concrete content could be seen in section 2.3. Because

of the mechanism of “error feedback connection”, BPNN has the good self-correcting capability for big error. So, BPNN has relatively lower requirements on input value than SVR. So long as the change of input

**Table 11**

Prediction error with input value of thermophysical properties of working fluid.

Model	Output	BORC		RORC		IORC		CRIORC	
		MRE/%	R <sup>2</sup>						
BPNN	$\eta_{th}$	3.2059	0.9883	2.4563	0.9906	2.5527	0.9907	2.5943	0.9763
	$\eta_{ex}$	2.8767	0.9832	3.1358	0.9815	5.5035	0.9507	2.4248	0.9709
SVR	$\eta_{th}$	2.4441	0.9947	1.2873	0.9967	1.8720	0.9971	1.6602	0.9861
	$\eta_{ex}$	2.7682	0.9901	1.5661	0.9932	2.4377	0.9919	1.8585	0.9758

value could correctly correspond to the change of output value, BPNN could make relatively accurate prediction after training. Like the working fluid number 1,2,3... in this paper, they correctly correspond to the change of output value (just not detailed enough in this way). And SVR algorithm is more suitable for predicting output value corresponded with explicit equation, which requires the input value and output value to satisfy some calculation relationship. Because of its unique regression mechanism ("interval band"), SVR will be more accurate when it obtains the detailed input values associated with the calculating equations. It is also the main reason for the improvement of prediction results of SVR after replacing number by thermodynamics parameters. And prediction error of improved SVR is smaller than BPNN. In conclusion, the two models have their own advantages and disadvantages, but the error of the prediction results of them in this paper is all in the acceptable range.

Based on the above prediction results, it could be suggested that for the thermal efficiency and exergy efficiency of BORC, RORC, IORC and CRIORC, BPNN and SVR models could achieve combined prediction including various working fluids as input value, and the prediction results are relatively accurate.

### 3.3. Reverse prediction for ORC operating parameters

After realizing the accurate prediction of thermal efficiency and exergy efficiency, this paper attempts to carry out the reverse prediction of cycle operating parameters. That is, thermal efficiency and exergy efficiency will be converted into the input value, and single or multiple cycle operating parameters as the output value to predict. In this paper, BORC was taken as an example to carry out reverse prediction for cyclic parameters.

#### 3.3.1. Prediction for evaporating pressure

BPNN and SVR models were used to predict the evaporating pressure. The input values include heat source temperature, pinch point temperature in the evaporator, degree of superheat, degree of supercooling, condensing temperature, thermal efficiency and exergy efficiency. The output value is evaporating pressure. Error values of prediction results are listed in Table 12.

It could be observed that for each working fluid, the MRE of BPNN basically kept between 2% and 6%, and the MRE of SVR basically kept between 2% and 4%. The prediction results of BPNN and SVR model for evaporating pressure were both relatively accurate. And the prediction error of SVR model was slightly smaller than BPNN.

#### 3.3.2. Prediction for evaporating pressure and heat source temperature

BPNN and SVR models were used to predict the evaporating pressure and heat source temperature. The input values include pinch point temperature, degree of superheat, degree of supercooling, condensing temperature, thermal efficiency and exergy efficiency, and the output values are evaporating pressure and heat source temperature. Error values of prediction results are listed in Table 13.

It could be observed that for each working fluid, the MRE of BPNN

for evaporating pressure basically kept between 2% and 6%, and the MRE for heat source temperature basically kept within 1%. The MRE of SVR for evaporating pressure basically maintained between 2% and 4%, and MRE of heat source temperature maintained within 1%. The prediction results of BPNN and SVR models for evaporating pressure and heat source temperature were both relatively accurate. In conclusion, in terms of predicted values of evaporating pressure and heat source temperature in reverse prediction, the prediction errors of SVR model are smaller than BPNN.

Based on the above prediction results, it could be suggested that for the BORC, BPNN and SVR models could achieve reverse prediction of single or multiple cycle parameters, and the prediction results are relatively accurate. The realization of reverse prediction has certain guiding significance for researchers to analyze and design ORC.

## 4. Parameter analysis and multi-objective optimization

In order to further verify the accuracy of prediction results of BPNN and SVR models, sensitivity analysis was carried out on some cycle parameters in this paper to verify whether the change rules of thermal efficiency and exergy efficiency with cycle parameters were consistent.

Taking RORC as example, the change rule of thermal efficiency and exergy efficiency with evaporating pressure for each working fluid was analyzed, and the simulation values and the prediction values of BPNN and SVR were compared, which was shown in Fig. 17. It could be seen that for each working fluid, the thermal efficiency and exergy efficiency of the simulation value increased with the increase of the evaporating pressure; for seven working fluids, the thermal and exergy efficiency of R141b, R11, R123, R245ca, R245fa, R114, R236ea decreased in turn. R141b has the best performance and R236ea has the worst performance in terms of thermal efficiency and exergy efficiency. Based on sensitivity analysis of prediction values of BPNN and SVR, it could be seen from the figure that since the reason of the prediction error, the working fluid curves changes from relatively smooth curves to lines with small fluctuation. But overall, for each working fluid, the thermal efficiency and exergy efficiency of the prediction value still increase with the increase of evaporating pressure, and the difference of performance of the working fluids is also basically consistent with the simulation values. This is consistent with the theoretical explanation of the thermodynamic analysis in Section 2.2.1, which further supports the results obtained from the prediction model.

Taking R141b as example, the change rule of thermal efficiency and exergy efficiency of BORC, RORC, IORC and CRIORC with evaporating pressure were analyzed, and the simulation value, the prediction value of BPNN and SVR, which was shown in Fig. 18. It could be seen that for four kinds of ORC configurations, thermal efficiency and exergy efficiency of the simulation values increase with the increase of the evaporating pressure. Comparatively, the thermal and exergy efficiency of CRIORC, IORC, BORC and RORC decreased in turn respectively. Under the condition that reheating pressure ratio is 0.15, CRIORC has the best performance and RORC has the worst performance in terms of thermal efficiency and exergy efficiency. Specifically, since the reheating

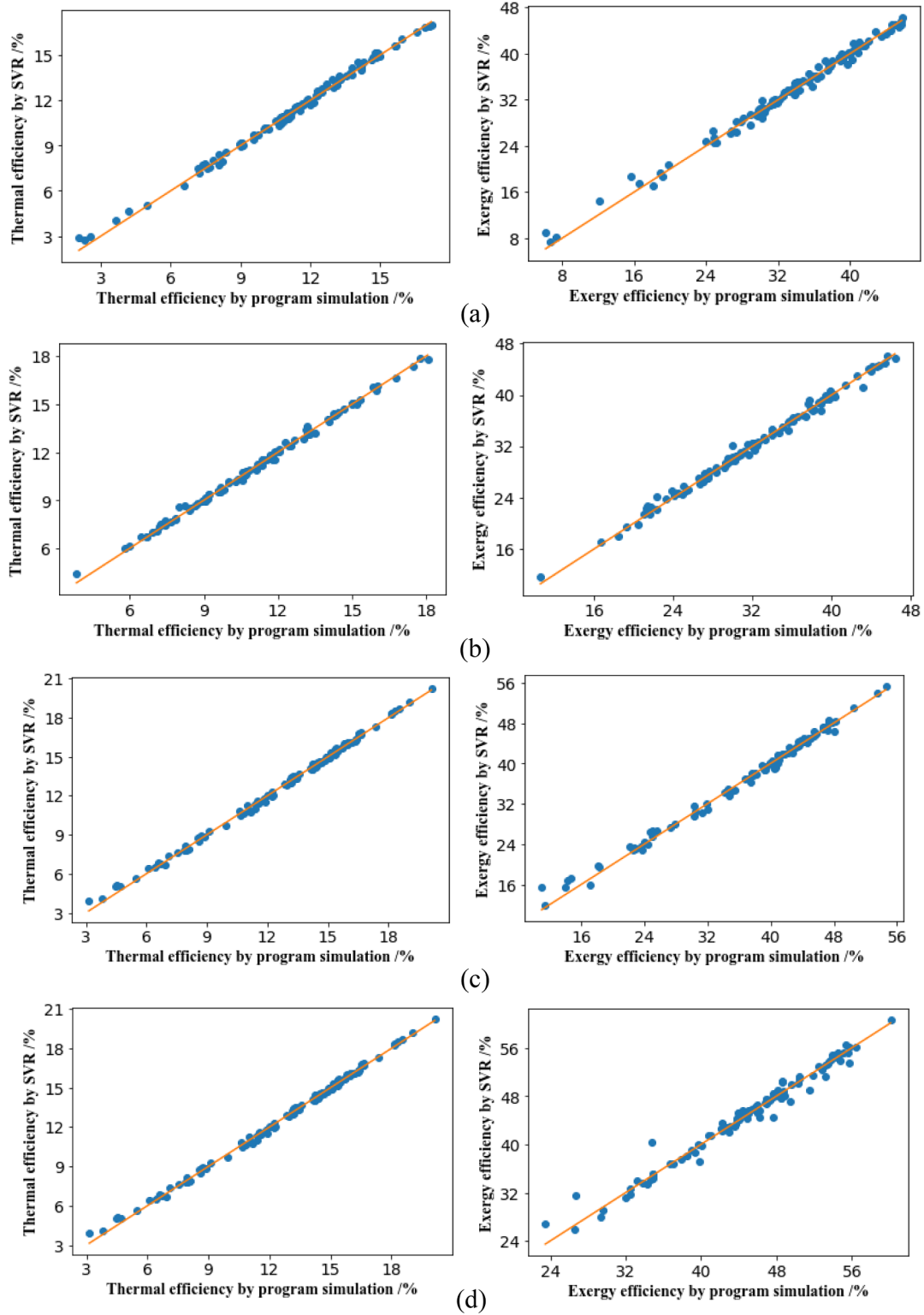


Fig. 16. Prediction result by SVR for thermal(left) and exergy(right) efficiency of BORC(a), RORC(b), IORC(c), CRIORC(d).

pressure ratio selected in this figure is not appropriate enough, the thermal and exergy efficiency of RORC are reduced slightly compared with BORC. However, the work per kilogram of working fluid increases (do work twice). When IORC is introduced into RORC, CRIORC that is the combination of RORC and IORC reduces the cycle average

temperature difference and the heat transfer temperature difference in the heat exchanger, significantly improving the thermal efficiency and exergy efficiency, and it also could increase the work per kilogram of working fluid. Same as the mentioned above, based on sensitivity analysis of prediction values of BPNN and SVR, it could be observed

**Table 12**

Prediction error for evaporating pressure.

Working Fluid	BPNN		SVR	
	MRE/%	R <sup>2</sup>	MRE/%	R <sup>2</sup>
R141b	3.9402	0.9899	3.0513	0.9898
R236ea	5.9869	0.9603	3.0981	0.9930
R245fa	3.4016	0.9920	3.0316	0.9942
R245ca	5.6962	0.9736	4.1363	0.9905
R123	5.9303	0.9700	3.3703	0.9865
R114	2.4643	0.9915	2.9839	0.9946
R11	2.6445	0.9933	2.8523	0.9911

**Table 13**

Prediction error for evaporating pressure and heat source temperature.

Model	Working fluid	<i>P</i> <sub>eva</sub>		<i>T</i> <sub>h</sub>	
		MRE/%	R <sup>2</sup>	MRE/%	R <sup>2</sup>
BPNN	R141b	5.0012	0.9698	0.9208	0.9601
	R236ea	4.1943	0.9794	0.5412	0.9768
	R245fa	2.6869	0.9942	0.7043	0.9604
	R245ca	6.9971	0.9428	0.4556	0.9859
	R123	3.1406	0.9883	0.6093	0.9804
	R114	6.2548	0.9584	0.3634	0.9913
	R11	5.7261	0.9760	0.7337	0.9666
SVR	R141b	2.9935	0.9856	0.7201	0.9785
	R236ea	3.4753	0.9896	0.6166	0.9765
	R245fa	3.2683	0.9923	0.6241	0.9791
	R245ca	3.2371	0.9895	0.6457	0.9772
	R123	3.7923	0.9796	0.5045	0.9868
	R114	2.3502	0.9940	0.5745	0.9800
	R11	2.6796	0.9962	0.5850	0.9808

that since the reason of the prediction error, the curves changes from relatively smooth curves to lines with small fluctuation. But overall, for each ORC configuration, the thermal efficiency and exergy efficiency of the prediction value still increase with the increase of evaporating pressure, and the difference of performance of the ORC configurations is also basically consistent with the simulation values. This is consistent with the above analysis and thermodynamic analysis in Section 2.2.1, which further supports the results obtained from the prediction model.

The above sensitivity analysis further verified the accuracy of the prediction results of BPNN and SVR. It is important to note that not only evaporating pressure has an effect on cycle performance, but other cycle operating parameters also have the different effect on thermal efficiency and exergy efficiency as shown in Figs. 19–21, and it should be noted that they are drawn by simulation data of thermodynamic model. Fig. 19 shows the effect of degree of superheat and reheat pressure ratio on thermal efficiency and exergy efficiency in RORC. It could be seen from the figure that both thermal efficiency and exergy efficiency increase with the increase of degree of superheat and reheat pressure ratio. And the change trend of thermal efficiency gradually slows down with the increase of reheat pressure ratio. The effect of degree of superheat on thermal efficiency and exergy efficiency is smaller than reheat pressure ratio. Although the effective degree of them is different, the thermal efficiency and exergy efficiency are jointly affected by them. Higher degree of superheat and reheat pressure ratio could achieve higher thermal efficiency and exergy efficiency in the range of figure.

Fig. 20 shows the effect of superheat and condensation temperature on thermal efficiency. It could be seen from the figure that the thermal efficiency decreases with the increase of the condensing temperature and degree of supercooling, and basically changes linearly, indicating

that the lower condensing temperature and degree of supercooling could achieve larger thermal efficiency.

Fig. 21 shows the effect of evaporating pressure and heat source temperature on exergy efficiency. It could be seen from the figure that exergy efficiency increases with the increase of evaporating pressure, and the increasing trend is gradually flat. The exergy efficiency decreases with the increase of the heat source temperature, so higher evaporating pressure and lower heat source temperature could achieve larger exergy efficiency.

Based on the above sensitivity analysis, cycle operating parameters jointly affected the thermal and exergy efficiency. Sensitivity analysis made the influence rule of each parameter on cycle performance clearer, but it was not comprehensive enough to get the maximum thermal efficiency, maximum exergy efficiency simultaneously and corresponding optimal operating parameters of ORC. In this case, multi-objective optimization is needed for thermal efficiency and exergy efficiency. In this study, RORC was still taken as an example to conduct multi-objective optimization for each working fluid by genetic algorithm, and the optimization was based on the thermodynamic model, BPNN model and SVR model respectively. Two prediction models, BPNN and SVR, were used as proxy models for thermodynamic models, which means that in the optimization, the calculation process of thermodynamic model is replaced by the prediction process of BPNN and SVR models. Optimization objective functions could be expressed as:

$$\max(\eta_{\text{th}}) = f(T_h, P_{\text{eva}}, T_{\text{sh}}, T_{\text{con}}, \Delta T_{\text{ppe}}, \lambda) \quad (31)$$

$$\max(\eta_{\text{ex}}) = f(T_h, P_{\text{eva}}, T_{\text{sh}}, T_{\text{con}}, \Delta T_{\text{ppe}}, \lambda) \quad (32)$$

The range of operating parameters is as follow:

$$400 \leq T_h \leq 480K \quad (33)$$

$$500 \leq p_{\text{eva}} \leq 3500 \text{kPa} \quad (34)$$

$$0 \leq T_{\text{sh}} \leq 21K \quad (35)$$

$$308.15K \leq T_{\text{con}} \leq 318.15K \quad (36)$$

$$5 \leq \Delta T_{\text{ppe}} \leq 20K \quad (37)$$

$$0.1 \leq \lambda \leq 0.6 \quad (38)$$

Generally, before the decision process, the Pareto frontier of the objective functions will be obtained for the multi-objective optimization. The optimal solution set on the frontier shows the tradeoff solutions between the objective functions. For example, Fig. 22 shows the Pareto frontier of multi-objective optimization based on the thermodynamic model for seven working fluids in this study. Each point in the figure is the optimal combination of thermal efficiency and exergy efficiency of RORC, that is, each point on the Pareto frontier is the optimal solution under different operating conditions.

After the Pareto frontier is obtained, the decision needs to be made to obtain the global optimal solution. To illustrate intuitively, in the decision process, this paper adopts the same weight for the two objective functions and then converts them into single-objective optimization. The objective function is:

$$F(T_h, P_{\text{eva}}, T_{\text{sh}}, T_{\text{con}}, \Delta T_{\text{ppe}}, \lambda) = 0.5 \cdot \eta_{\text{th}} + 0.5 \cdot \eta_{\text{ex}} \quad (39)$$

Based on above objective function, the final global optimization results were listed in Table 14. It could be observed that the optimization results based on the thermodynamic model, BPNN model and SVR model are very close. So, a new approach to achieve relatively rough optimization based on above processes was proposed. This method uses the accurate prediction model as a proxy model instead of thermodynamic model to output objective function value to realize multi-objective optimization. Firstly, the use of a proxy model allows us

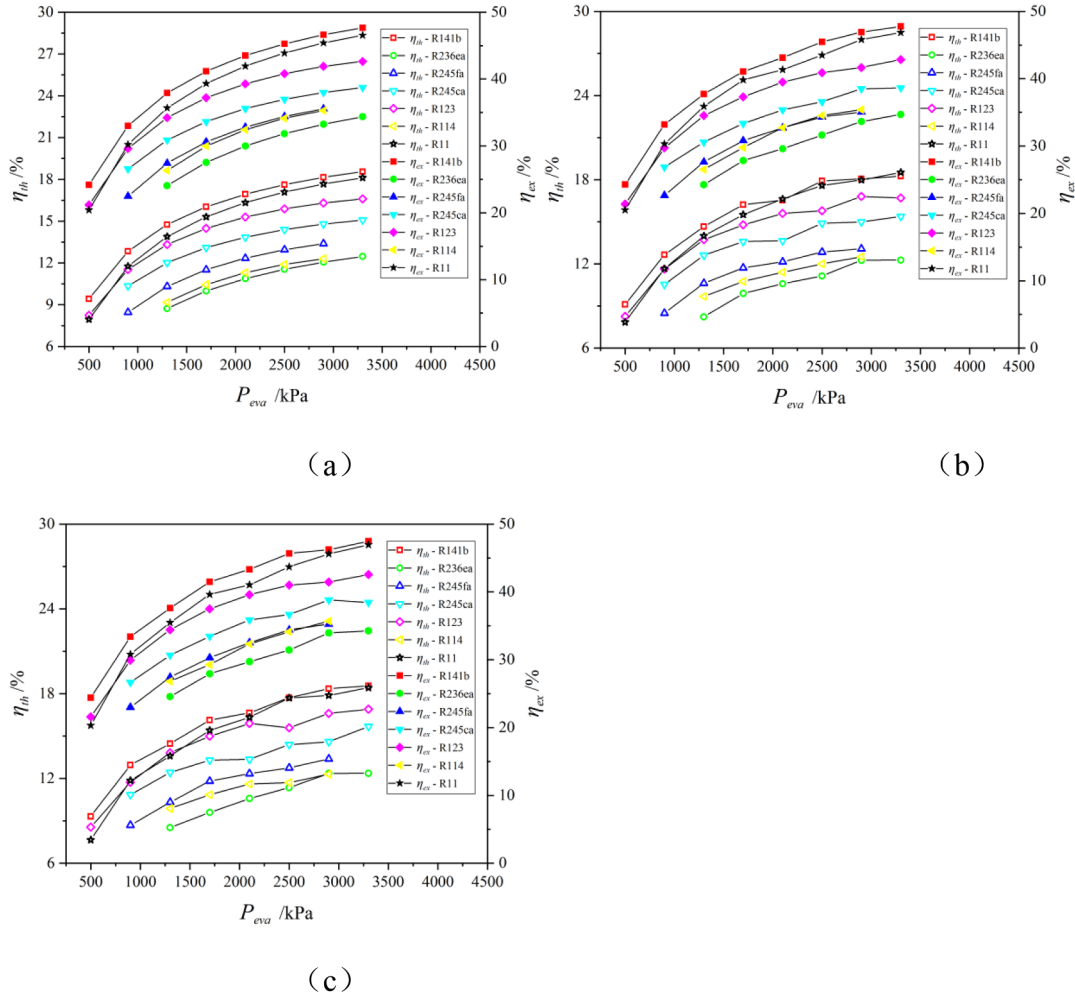


**Fig. 17.** The effect of evaporating pressure on thermal and exergy efficiency with different working fluids by simulation(a), BPNN(b) and SVR(c).

not to have to write complex simulation programs for research another time. And then, because the time of prediction process is much shorter than the calculation process of the thermodynamic model, the optimization is naturally faster. Therefore, this method could obtain an optimal solution simply and quickly while ensuring certain accuracy, which could replace the traditional multi-objective optimization based on the thermodynamic model to some extent. It is promising that this method could provide some pre-guidance in engineering practice when researchers analyze and design ORC.

Furthermore, in addition to the advantages mentioned above, some possible limitations of this method also need to be discussed to realize the further improvement in future work:

- 1) The “black box” model obtained by Machine Learning could only reflect a general causality between input and output, and couldn’t explain the internal operating mechanism of ORC systems compared with traditional methods resulting in that it may be more suitable for engineering applications than theoretical research in the future.
- 2) Compared with the simulation method, the advantages and disadvantages between various Machine Learning models were not overwhelming. It should be analyzed according to the specific problem, especially whether the provided features were detailed enough to fit different models.
- 3) The data in this paper come from the simulation of ideal ORC rather

than experiments, however, it could reasonably be inferred from this work that this method will have a promising guiding significance for engineering practice after further training of practical data.

## 5. Conclusions

This study proposed a new comprehensive method applying Machine Learning into ORC research for prediction and optimization and the results showed its good feasibility and effectiveness. Based on this work, the main specific conclusions were summarized as follows:

- 1) The best parameters of the BPNN and SVR models in this paper were determined respectively through error analysis of the prediction results. Comparatively, the time of simulation for 40,000 groups of BORC data was about 20 and 8 times respectively as longer as prediction of BPNN and SVR.
- 2) The thermal efficiency and exergy efficiency of four ORC configurations for each working fluid were accurately predicted. MRE of BPNN generally maintained about 1%-5%, and MRE of SVR was about 1%-2%. And the later sensitivity analysis based on the simulation and prediction data further verified this accuracy.
- 3) For the combined prediction for seven working fluids, two kinds of input forms of working fluids were proposed in this paper, which were numbered input and thermophysical parameters

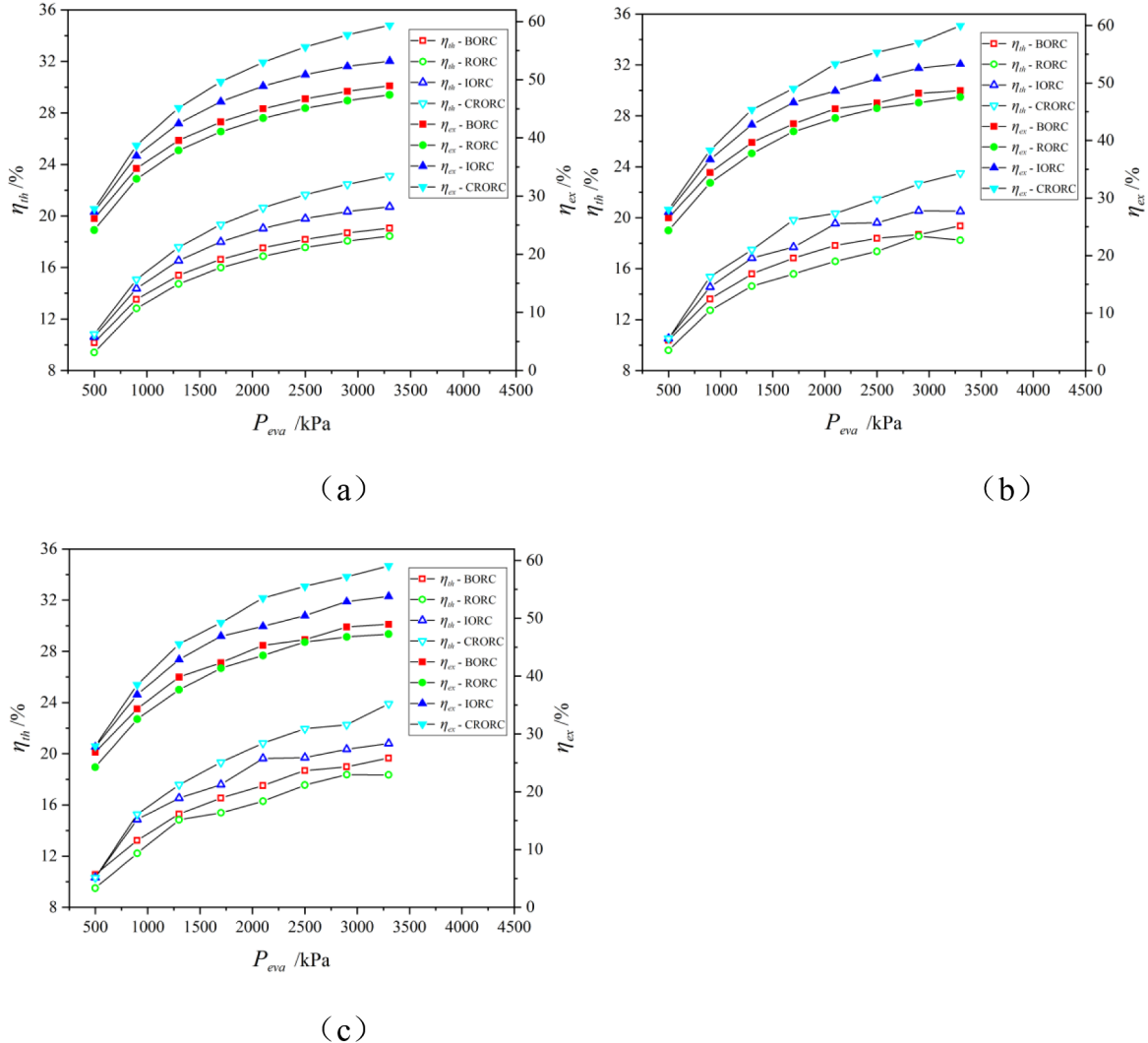


**Fig. 18.** The effect of evaporating pressure on thermal and exergy efficiency with different ORC configurations by simulation(a), BPNN(b) and SVR(c).

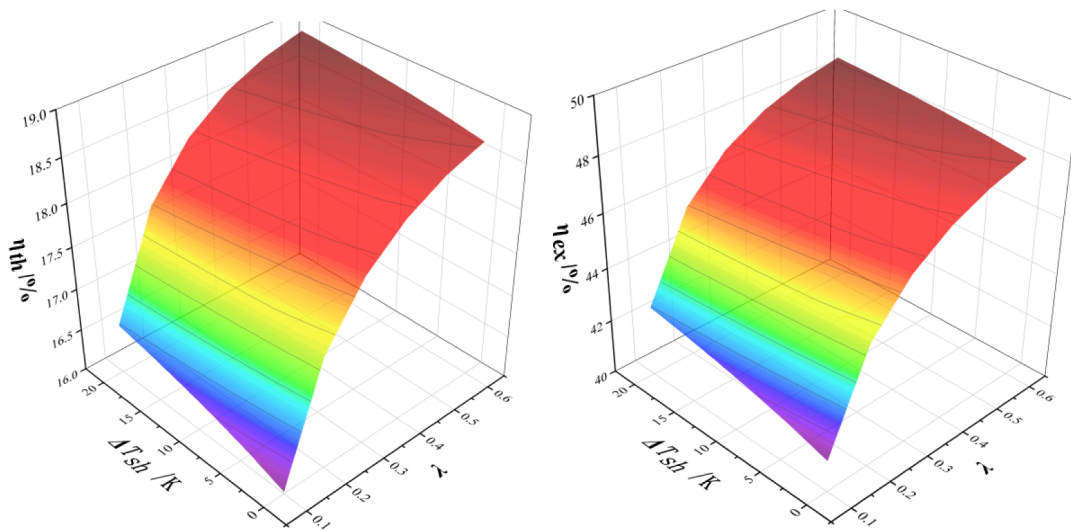


**Fig. 19.** The effect of the degree of superheat and reheat pressure ratio on thermal(left) and exergy(right) efficiency.

input. The latter could significantly improve the prediction effect compared with the former. In addition, the relatively accurate reverse prediction for cycle operating parameters was realized, such as

evaporating pressure, heat source temperature.

- 4) To sum up, SVR can provide higher accuracy than BPNN when the data is detailed and the input form is appropriate, otherwise the

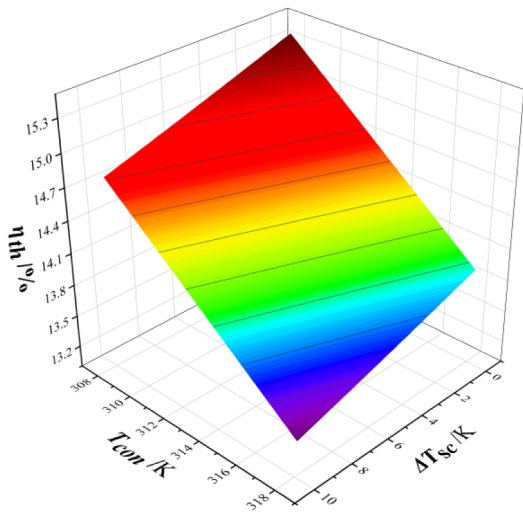


Fig. 20. The effect of degree of supercooling and condensing temperature on thermal efficiency.

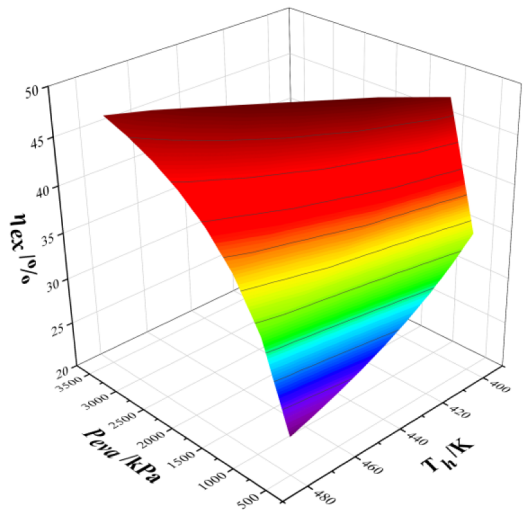


Fig. 21. The effect of evaporating pressure and heat source temperature on exergy efficiency.

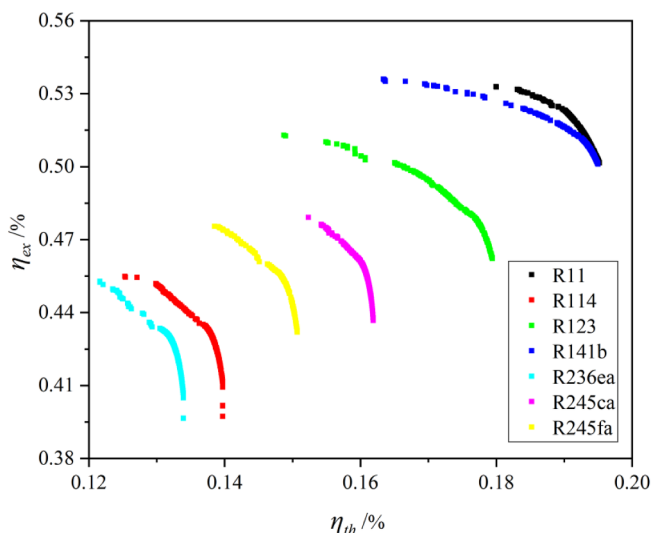


Fig. 22. Pareto frontier of multi-objective optimization for seven working fluids.

**Table 14**  
Optimization result.

	Thermodynamic model	BPNN model	SVR model
Working fluid	R11	R11	R11
$P_{eva}$ /kPa	2886.59	2887.58	2888.26
$T_h$ /K	447.56	447.02	448.64
$T_{con}$ /K	308.15	308.16	308.15
$\Delta T_{pp}$ /K	5.00	5.02	5.01
$T_{sh}$ /K	0.00	0.00	0.00
$\lambda$	0.60	0.59	0.60
$\eta_{th}$	18.34	18.22	18.03
$\eta_{ex}$	53.16	54.02	53.82

BPNN is more reliable. In other words, BPNN is more robust and has relatively loose requirement for data compared with SVR.

- 5) In the optimization process, the Machine Learning model was used as the proxy model to replace the thermodynamic model. And the results showed that this approach could realize the ORC performance optimization quickly, accurately and effectively, which could replace the traditional optimization based on the thermodynamic model.

## 6. Data availability

To facilitate reproducibility and data reuse for readers, several parts of databases and models in this paper are provided as supplementary materials, including database of BORC with R141b, database of BORC with combined working fluids, BPNN and SVR models for individual prediction of BORC with R141b, and BPNN and SVR models for combined prediction of BORC. It should be noted that models are operated in TensorFlow framework based on Anaconda 2019.10 version of Python 3.6 version in this paper.

## CRediT authorship contribution statement

**Wei Wang:** Conceptualization, Methodology, Software, Validation, Writing - original draft, Writing - review & editing. **Shuai Deng:** Conceptualization, Methodology, Writing - review & editing, Supervision, Funding acquisition. **Dongpeng Zhao:** Conceptualization, Software, Writing - review & editing. **Li Zhao:** Project administration, Funding acquisition, Supervision. **Shan Lin:** Data curation, Investigation. **Mengchao Chen:** Investigation, Supervision.

## Declaration of Competing Interest

The authors declare that they have no known competing financial interests or personal relationships that could have appeared to influence the work reported in this paper.

## Acknowledgement

This work is supported by the National Key Research and Development Plan of China under Grant No. 2018YFB1501004.

## References

- [1] Chen LX, Hu P, Sheng CC, Xie MN. A novel compressed air energy storage (CAES) system combined with pre-cooler and using low grade waste heat as heat source. Energy 2017;131:259–66.
- [2] Chintala V, Kumar S, Pandey JK. A technical review on waste heat recovery from compression ignition engines using organic Rankine cycle. Renew Sustain Energy Rev 2018;81:493–509.
- [3] Eller T, Heberle F, Brüggemann D. Second law analysis of novel working fluid pairs for waste heat recovery by the Kalina cycle. Energy 2017;119:188–98.
- [4] Nader WB, Mansour C, Dumand C, Nemer M. Brayton cycles as waste heat recovery systems on series hybrid electric vehicles. Energ Convers Manage 2018;168:200–14.
- [5] Wang M, Becker TM, Schouten BA, Vlugt TJH, Infante Ferreira CA. Ammonia/ionic liquid based double-effect vapor absorption refrigeration cycles driven by waste

- heat for cooling in fishing vessels. *Energ Convers Manage* 2018;174:824–43.
- [6] Wang K, Sanders SR, Dubey S, Choo FH, Duan F. Stirling cycle engines for recovering low and moderate temperature heat: a review. *Renew Sustain Energy Rev* 2016;62:89–108.
- [7] Xu Y, Guo F, Song M, Jiang N, Wang Q, Chen G. Exergetic and economic analyses of a novel modified solar-heat-powered ejection-compression refrigeration cycle comparing with conventional cycle. *Energ Convers Manage* 2018;168:107–18.
- [8] Yang F, Zhang H, Song S, Bei C, Wang H, Wang E. Thermoeconomic multi-objective optimization of an organic Rankine cycle for exhaust waste heat recovery of a diesel engine. *Energy* 2015;93:2208–28.
- [9] Quoilin S, Broek MVD, Declaye S, Dewallef P, Lemort V. Techno-economic survey of organic rankine cycle (ORC) systems. *Renew Sustain Energy Rev* 2013;22:168–86.
- [10] Usman M, Imran M, Yang Y, Park BS. Impact of organic Rankine cycle system installation on light duty vehicle considering both positive and negative aspects. *Energ Convers Manage* 2016;112:382–94.
- [11] Tang L, Wang YP, Yang P, Weng YW. Experiments of low-grade heat organic rankine cycle power generation optimal load characteristics. *Trans Tech Publications Ltd*; 2014. p. 481–5.
- [12] Xu W, Zhang J, Zhao L, Deng S, Zhang Y. Novel experimental research on the compression process in organic Rankine cycle (ORC). *Energ Convers Manage* 2017;137:1–11.
- [13] Dumont O, Parthoens A, Dickes R, Lemort V. Experimental investigation and optimal performance assessment of four volumetric expanders (scroll, screw, piston and roots) tested in a small-scale organic Rankine cycle system. *Energy* 2018;1119–27.
- [14] Bufl EA, Camporeale S, Fornarelli F, Fortunato B, Pantaleo AM, Sorrentino A, et al., “Parametric multi-objective optimization of an Organic Rankine Cycle with thermal energy storage for distributed generation,” (Elsevier Ltd, 2017), pp. 429–436.
- [15] Zhai L, Xu G, Wen J, Quan Y, Fu J, Wu H, et al. An improved modeling for low-grade organic Rankine cycle coupled with optimization design of radial-inflow turbine. *Energ Convers Manage* 2017;153:60–70.
- [16] Zhang Y, Deng S, Zhao L, Lin S, Ni J, Ma M, et al. Optimization and multi-time scale modeling of pilot solar driven polygeneration system based on organic Rankine cycle. *Appl Energ* 2018;222:396–409.
- [17] Chatzopoulou MA, Markides CN. Thermodynamic optimisation of a high-electrical efficiency integrated internal combustion engine – Organic Rankine cycle combined heat and power system. *Appl Energ* 2018;226:1229–51.
- [18] Ziviani D, Gusev S, Lecompte S, Groll EA, Braun JE, Horton WT, et al. Optimizing the performance of small-scale organic Rankine cycle that utilizes a single-screw expander. *Appl Energ* 2017;189:416–32.
- [19] Yang J, Sun Z, Yu B, Chen J. Experimental comparison and optimization guidance of R1233zd(E) as a drop-in replacement to R245fa for organic Rankine cycle application. *Appl Therm Eng* 2018;141:10–9.
- [20] Ghasemian E, Ehyaei MA. Evaluation and optimization of organic Rankine cycle (ORC) with algorithms NSGA-II, MOPSO, and MOEA for eight coolant fluids. *Int J Energy Environ Eng* 2018;9:39–57.
- [21] Bao J, Zhang R, Lin Y, Zhang N, Zhang X, He G. Simultaneous optimization of system structure and working fluid for the three-stage condensation Rankine cycle utilizing LNG cold energy. *Appl Therm Eng* 2018;140:120–30.
- [22] Sun F, Ikegami Y, Jia B, Arima H. Optimization design and energy analysis of organic rankine cycle in ocean thermal energy conversion. *Appl Ocean Res* 2012;35:38–46.
- [23] Liu M, Zhang X, Yang K, Wang B, Yan J. Comparison and sensitivity analysis of the efficiency enhancements of coal-fired power plants integrated with supercritical CO<sub>2</sub> Brayton cycle and steam Rankine cycle. *Energ Convers Manage* 2019;198.
- [24] Shan S, Zhou Z, Cen K. An innovative integrated system concept between oxy-fuel thermo-photovoltaic device and a Brayton-Rankine combined cycle and its preliminary thermodynamic analysis. *Energ Convers Manage* 2019;180:1139–52.
- [25] Bahari SS, Sameti M, Ahmadi MH, Haghighooyan MS. Optimisation of a combined Stirling cycle–organic Rankine cycle using a genetic algorithm. *Int J Ambient Energy* 2016;37:398–402.
- [26] Borboudakis G, Stergiannakos T, Frysali M, Klontzas E, Tsamardinos I, Froudakis GE. Chemically intuited, large-scale screening of MOFs by machine learning techniques. *Npj Comput Mater* 2017;3.
- [27] Meng Y, Pang H, Jiang Y, Zhou Q, Zheng T, Jin Q. Analysis of heat exchanger performance forecast based on the BP neural network. 2010. p. 1697–1701.
- [28] Zhi LH, Hu P, Chen LX, Zhao G. Multiple parametric analysis, optimization and efficiency prediction of transcritical organic Rankine cycle using trans-1,3,3,3-tetrafluoropropene (R1234ze(E)) for low grade waste heat recovery. *Energ Convers Manage* 2019;44:44–59.
- [29] Yang F, Cho H, Zhang H. Performance prediction and optimization of an organic rankine cycle using back propagation neural network for diesel engine waste heat recovery. *J Energy Resour Technol Trans ASME* 2019;141.
- [30] Dong S, Zhang Y, He Z, Deng N, Yu X, Yao S. Investigation of Support Vector Machine and Back Propagation Artificial Neural Network for performance prediction of the organic Rankine cycle system. *Energy* 2018;144:851–64.
- [31] Cherkassky V, Ma Y. Practical selection of SVM parameters and noise estimation for SVM regression. *Neural Networks* 2004;17:113–26.
- [32] Schmidhuber J. Deep Learning in neural networks: an overview. *Neural Networks* 2015;61:85–117.